COLLABORATIVE RESEARCH AND DEVELOPMENT (CR&D)

Delivery Order 0023: Molecular Simulation for Material Design Limits

Martin Schwartz

University of North Texas

NOVEMBER 2005
Final Report

STINFO COPY

AIR FORCE RESEARCH LABORATORY
MATERIALS AND MANUFACTURING DIRECTORATE
WRIGHT-PATTERSON AIR FORCE BASE, OH 45433-7750
AIR FORCE MATERIEL COMMAND
UNITED STATES AIR FORCE

NOTICE AND SIGNATURE PAGE

*//Signature//   //Signature//

RITA SCHOLES   ROBERT ENGHAUSER
Project Manager   Acting Chief
Business Operations Branch   Business Operations Branch
Integration and Operations Division   Integration and Operations Division
Materials and Manufacturing Directorate

REPORT DOCUMENTATION PAGE

1. REPORT DATE *(DD-MM-YY)*	2. REPORT TYPE	3. DATES COVERED *(From - To)*
November 2005	Final	01 May 2004 – 31 August 2005

4. TITLE AND SUBTITLE

COLLABORATIVE RESEARCH AND DEVELOPMENT (CR&D)
Delivery Order 0023: Molecular Simulation for Material Design Limits

5a. CONTRACT NUMBER
F33615-03-D-5801-0023

5b. GRANT NUMBER

5c. PROGRAM ELEMENT NUMBER
61202F

6. AUTHOR(S)

Martin Schwartz (University of North Texas)

5d. PROJECT NUMBER
4349

5e. TASK NUMBER
L0

5f. WORK UNIT NUMBER
4349L0VT

7. PERFORMING ORGANIZATION NAME(S) AND ADDRESS(ES)

By:

University of North Texas
Department of Chemistry
Denton, TX 76203

For:

Universal Technology Corporation
1270 North Fairfield Road
Dayton, OH 45432-2600

8. PERFORMING ORGANIZATION REPORT NUMBER

S-531-0023

9. SPONSORING/MONITORING AGENCY NAME(S) AND ADDRESS(ES)

Air Force Research Laboratory
Materials and Manufacturing Directorate
Wright-Patterson Air Force Base, OH 45433-7750
Air Force Materiel Command
United States Air Force

10. SPONSORING/MONITORING AGENCY ACRONYM(S)
AFRL/RXOB

11. SPONSORING/MONITORING AGENCY REPORT NUMBER(S)
AFRL-RX-WP-TR-2010-4082

12. DISTRIBUTION/AVAILABILITY STATEMENT
Approved for public release; distribution unlimited.

13. SUPPLEMENTARY NOTES
PAO Case Number: AFRL/WS 06-2355; Clearance Date: 01 Jan 2006. Research was completed in 2005.

14. ABSTRACT

This research in support of the Air Force Research Laboratory Materials and Manufacturing Directorate was conducted at Wright- Patterson AFB, Ohio during two summer sessions from 1 May 2004 through 31 Aug 2005. The research investigated the ability of Molecular Dynamics simulations to replicate the mechanical properties of Parmax self-reinforced polymers. This report presents details of the simulation, test procedures, and results.

15. SUBJECT TERMS
Molecular Dynamics simulation, self-reinforced polymers

16. SECURITY CLASSIFICATION OF:			17. LIMITATION OF ABSTRACT:	18. NUMBER OF PAGES	19a. NAME OF RESPONSIBLE PERSON (Monitor)
a. REPORT Unclassified	**b. ABSTRACT** Unclassified	**c. THIS PAGE** Unclassified	SAR	62	Rita Scholes
					19b. TELEPHONE NUMBER *(Include Area Code)* N/A

TABLE OF CONTENTS

I.   INTRODUCTION

A major goal of this study is to ascertain the ability of Molecular Dynamics simulations to replicate the mechanical properties of Parmax® self-reinforced polymers (SRPs). These polymers consist of chains of para- and meta- linked phenylene units with benzoyl group substituents.   In recent years, substituted polyphenylenes have emerged as a new class of compounds with excellent mechanical properties (high modulus, yield strength and hardness). They also display excellent thermal stabilities and processabilities (low T_g and soluble in many organic solvents).

Prior to initiating investigating the Parmax SRPs, we studied atactic Polypropylene (aPP), which is a glassy polymer with a well characterized glass transition temperature and reasonably well characterized mechanical properties.
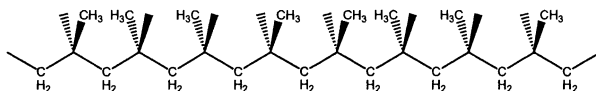
We used our simulations on this polymer to develop procedures necessary to determine the various mechanical moduli as well as the yield strength in amorphous polymeric systems.

Following the studies on aPP, we have chosen to investigate three commercially available benzoyl substituted polyphenylenes (Ultem-1000, Parmax-1200, Parmax-1500) [1] as well as unsubstituted poly(paraphenylene) [PPP] for comparison.

| Ultem-1000 | Parmax-1200 | Parmax-1500 | PPP |

1
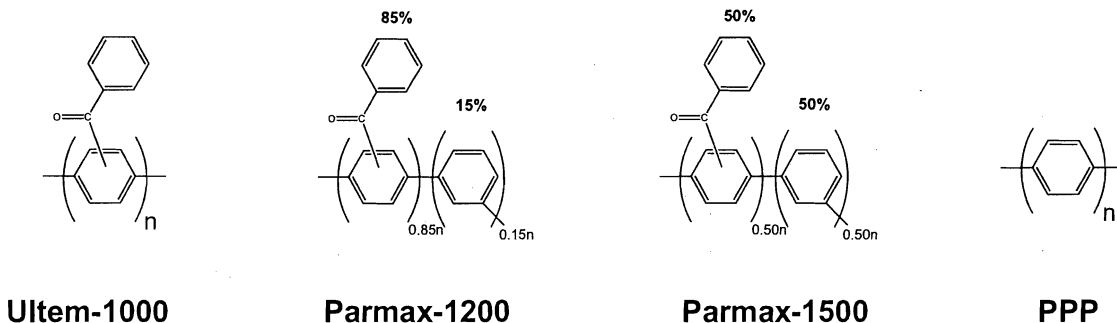
One notes from the structures that,like PPP, Ultem-1000 has 100% para linkages (as well as 2,3-benzoyl groups on all monomers). Parmax-1200 contains only 85% para linked phenylenes (and 85% benzoyl substitution), and Paramax-1500 is only 50% para linked (and 50% substitution).

Below, we give more details on the systems investigated (Sect. II), the computational methods used in the simulations (Sect. III), and then the computed vs. experimental properties, first of aPP and then of the Parmax SRPs (Sect. IV).

II.   SYSTEMS INVESTIGATED

With a goal towards developing the protocols required to compute accurate elastic moduli and yield stresses in amorphous polymers, initial investigations in Summer 2004, were performed on the well-studied glassy system, atactic polypropylene [aPP], which has the structure:
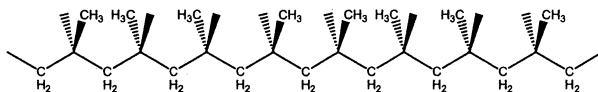
The molecular dynamics cells were comprised of three aPP oligomers, each containing 76 monomer units [689 total atoms, including H_3C- and $-H$ endcaps].

During Summer 2005, we have begun analogous investigations of three Parmax Self-Reinforced Polymers (SRPs): (A) Ultem-1000 [U-1000], (B) Parmax-1200 [PX-1200], (C) Parmax-1500 [PX-1500], in addition to the nonsubstituted analogue (D) Poly(paraphenylene) [PPP].

The MD cells were designed to contain a minimum of ≥1500 atoms and have cell lengths of at least 25 Å. These four systems were comprised of:

U-1000:   3 strands   25 monomers/strand   1656 total atoms

PX-1200:   3 strands   25 monomers/strand   1512 total atoms

PX-1500:   4 strands   25 monomers/strand   1608 total atoms

PPP: 6 strands   25 monomers/strand   1512 total atoms

III.   COMPUTATIONAL PROCEDURES

Simulations were performed using the *Accelrys*[2] Discover molecular dynamics program and associated software modules. The Accelrys COMPASS® [3-6] force field, designed to yield accurate values for both gas phase and liquid phase properties, was used for all the simulations. COMPASS is a completely atomistic Class II force field, and the potential energy function contains valence terms involving bond lengths, angles, and dihedrals + cross terms. As with other modern force-fields, there are also out-of-plane terms designed to maintain planarity in aromatic systems, including the phenyl rings present in all of the model systems investigated in this work. Other than terms in the potential energy function, no further constraints were applied to the molecules (i.e. bond-lengths, ring geometries, etc., were not frozen). As discussed in the original references,[3-6] the nonbond parameters were optimized to reproduce molar volumes and enthalpies of vaporization in a suite of test molecules under ambient conditions (usually 298 K and 1 atm. pressure), in which aromatic systems were represented by benzene and toluene.[5]

Cubic cells containing each model system were built via a Monte Carlo algorithm as implemented in the *Accelrys*[7] Amorphous Cell module. Following minimization to remove close contacts, the cells were heated to a temperature well above the glass transition temperature, T_g, and were equilbrated for XX ns using NPT dynamics. (Andersen thermostat[8] and Berendsen barostat[9]). All simulations were performed with periodic boundary conditions and 10 Å group-based cutoffs. The step size was 1 fs.

Equilibrated cells at lower temperatures were obtained by successive cooling at 50 K intervals down to 50 K, and equilibrating using NPT dynamics at each temperature. The equilibrated cell volumes from these runs were used to determine the density and specific volume at each temperature.

In order to acquire the tabular data necessary for the calculation of elastic moduli (stresses and strains in each cell direction), further NPT simulations were performed at each temperature using the the Parrinello-Rahman method (xx ref), in which an NPT simulation was performed with Parrinello pressure control and XX temperature control. The difference between this run and earlier NPT simulations is that the x,y and z dimensions of the box are permitted independently, allowing the calculation of strains (deformations) along the three cell axes. The initial box dimensions and atomic coordinates were taken from the final frame of the earlier equilibration runs. The simulation times were 1100 ps, and the first 100 ps were ignored in the calculation of elastic properties (*vide infra*).

For the determination of stress vs. strain curves, a BTCL script was written to perform a simulation in which (a) the stress in the x-direction was increased (usually in 50 bar increments) up to a maximum of ~2500 bar, with the time at each stress determined by the stress-rate (values of 5, 3 and 1 bar/ps were used). The procedure

was repeated with stresses in the y and then z directions. A Matlab script was then written to further analyze the results by averaging the stress-strain curves in the three experiments.

IV. RESULTS AND DISCUSSION

IVA. Atactic Polypropylene

In order to develop and test the procedures for determining properties of the Parmax SFPs, we chose to run MD simulations on a simpler polymer, atactic polypropylene (aPP). This system (a) is known to be completely completely amorphous (0% crystallinity), (b) has reasonably well characterized volumetric properties (density, thermal expansion coefficients and glass transition temperature),[10-12] and (c) its mechanical properties have been investigated both experimentally[13] and via earlier MD simulations.[14] Two independent sets of simulations, using different randomly built amorphous cells, were performed on aPP. The average properties (and mean deviations) are presented below.

A.1 Volumetric Properties of aPP

Contained in Table 1A are the available experimental specific volumes of aPP[11-13] as well as volumes (computed from NPT runs) for one of the simulations over a range of temperature from 50 K - 500 K. Calculated specific volumes from the two simulations were generally very close, and agreed to within ≤0.5 %, with the largest differences ≤1.3%. Calculated and experimental volumes are also displayed in Fig. 1 (filled and open symbols, respectively). One observes from both table and figure that there is very close agreement between computed and experimental values, to within ≤0.7% in the high temperature, rubbery regime. The authors are not aware of any experimental densities in the glass phase, below T_g.

Lines tangent to the computed volumes in the glass and rubbery phases were determined from the four lowest and highest temperatures, respectively, and are displayed as dotted lines in Fig. 1 (displaced downward for clarity of presentation). Using the standard procedure, the glass transition temperature was determined by the intercept of the two lines. From the data in the figure, it was found for the first of the two simulations that $T_g(cal) = 297$ K; the second run (not shown) yielded $T_g(cal) = 289$ K. The average computed glass transition temperature, 293 K, is 16-18 K above two recent determinations[11,12] but 43 K above an earlier reported value. It is not surprising that the computed value of T_g is higher than experimental values. This is generally found in MD simulations as a result of the extremely high effective cooling rates, which elevate the computed phase transition temperature.

Shown also in Table 1A and Fig. 1 (dashed curve) are specific volumes calculated from from QSPR correlations, Eqs. [A.1] and [A.2], with required parameters $V(298)$ taken from experiment (Table 1A) and $\alpha_R(298)$ determined from Eq. [A.4] (using $T_g = 275$ K). As shown in the figure the volumes estimated from QSPR agree extremely well with both experiment and the MD simulations (to within at high temperatues, and are in reasonable qualitative agreement with $V_{sp}(MD)$ in the low temperature, glassy regime (deviations average 1%-2% over the range of temperatures in the glass). Interestingly, the glass transition temperature predicted from the intercept of lines drawn tangent to the QSPR volumes at the extremes in temperature yield a value, $T_g = 277$ K, in excellent agreement with the more recent experiments.[11,12]

The slopes of the lines tangent to the computed specific volumes (Fig. 1), $(\partial V_{sp}/\partial T)_P$, can also be used to determine the thermal expansion coefficients in the glass and rubber phases:

$$\alpha = \frac{1}{V_{sp}} \left(\frac{\partial V_{sp}}{\partial T} \right)_P \qquad\qquad [1]$$

Eq. [1] was used (with average volumes over the temperature range spanned by each tangent line) to determine expansion coefficients, α_G and α_R, in the two phases. The average values (and mean deviations) for the two simulations are given in Table 1B, together with available experimental results. It may be that α_G(MD) lies very close to the middle of the range of expansion coefficients published for aPP. The agreement between α_R(MD) and α_R(Exp) is also good. The computed expansion coefficient lies within 5%-10% of the three experimental values in the high temperature phase.

Thermal expansion coefficients computed from tangent lines to the QSPR volumes (not shown in the figure) are contained in the last column of Table 1A. Alternatively, one can use the empirical correlations between $\alpha(T)$ and T_g (Eqs. [A.3] and [A.4]). For temperatures representing the average of the low and high temperature regimes, values of α_G and α_R (125 K and 425 K, respectively), obtained from the equations are in excelllent agreement with those computed from the equations and from slopes of the tangent lines. The difference between QSPR and MD values of α_R are insignificant (differing by < 5%). There is a more substantial difference between α_G(MD) and α_G(QSPR) [. Unfortunately, because of the large range in experimental determinations,[11-13] the relative accuracy of the two estimation methods cannot be ascertained.

A.2 Elastic Moduli of aPP

The six elements of the strain tensor (σ_i) are related to the six stress components (ε_j) by the "stiffness matrix" (C_{ij}) via the transformation:[15,16]

$$\begin{bmatrix} \sigma_1 \\ \sigma_2 \\ \sigma_3 \\ \sigma_4 \\ \sigma_5 \\ \sigma_6 \end{bmatrix} = \begin{bmatrix} C_{11} & C_{12} & C_{13} & C_{14} & C_{15} & C_{16} \\ C_{21} & C_{22} & C_{23} & C_{24} & C_{25} & C_{26} \\ C_{31} & C_{32} & C_{33} & C_{34} & C_{35} & C_{36} \\ C_{41} & C_{42} & C_{43} & C_{44} & C_{45} & C_{46} \\ C_{51} & C_{52} & C_{53} & C_{54} & C_{55} & C_{56} \\ C_{61} & C_{62} & C_{63} & C_{64} & C_{65} & C_{66} \end{bmatrix} \begin{bmatrix} \varepsilon_1 \\ \varepsilon_2 \\ \varepsilon_3 \\ \varepsilon_4 \\ \varepsilon_5 \\ \varepsilon_6 \end{bmatrix} \qquad [2]$$

Because the stiffness matrix is symmetric (i.e. $C_{ji} = C_{ij}$), there can be as many as 21 independent elements. However, the symmetry present in most systems will reduce the number of independent terms dramatically. Of specific interest to us is the matrix for amorphous, isotropic systems, in which case all matrix elements can be cast in terms of the two Lamé coefficients, λ and μ, and is of the form:[15,16]

$$\begin{bmatrix} \sigma_1 \\ \sigma_2 \\ \sigma_3 \\ \sigma_4 \\ \sigma_5 \\ \sigma_6 \end{bmatrix} = \begin{bmatrix} \lambda + 2\mu & \lambda & \lambda & 0 & 0 & 0 \\ \lambda & \lambda + 2\mu & \lambda & 0 & 0 & 0 \\ \lambda & \lambda & \lambda + 2\mu & 0 & 0 & 0 \\ 0 & 0 & 0 & \mu & 0 & 0 \\ 0 & 0 & 0 & 0 & \mu & 0 \\ 0 & 0 & 0 & 0 & 0 & \mu \end{bmatrix} \begin{bmatrix} \varepsilon_1 \\ \varepsilon_2 \\ \varepsilon_3 \\ \varepsilon_4 \\ \varepsilon_5 \\ \varepsilon_6 \end{bmatrix} \qquad [3]$$

In turn, the tensile modulus (E), bulk modulus (B), shear modulus (G) and Poisson's ratio (ν) are functions of the Lamé coefficients, and given by:

$$E = \mu\left(\frac{3\lambda + 2\mu}{\lambda + \mu}\right) \qquad [4]$$

$$B = \lambda + \frac{2}{3}\mu \qquad [5]$$

8

$$G = \mu \tag{6}$$

$$\nu = \frac{1}{2}\frac{\lambda}{\mu + \lambda} \tag{7}$$

Probably the most versatile method for utilizing a Molecular Dynamics simulation to determine elements of the stiffness matrix and, hence, the elastic moduli, is the "fluctuation method," introduced by Parrinello and Rahman.[17] They proved the individual elements of **C** are related to correlations in strain tensor elements via the relation:

$$C_{ij} = \frac{kT}{\langle V \rangle}\langle \varepsilon_i \varepsilon_j \rangle \tag{8}$$

where T and T and <V> are the temperature (K) and averaged cell volume. $\langle \varepsilon_i \varepsilon_j \rangle$ represents the average of strain tensor components over all frames in the simulation's production run. More recently, Gusev et al.[18] pointed out that the original fluctuation expression for C_{ij} is slowly convergent, oftentimes requiring very lengthy simulations. They proposed the the following alternative formula for C_{ij}, which converges more rapidly:

$$C_{ij} = \sum_k \frac{\langle \varepsilon_i \sigma_k \rangle}{\langle \varepsilon_k \varepsilon_j \rangle} \tag{9}$$

To obtain the requisite stress and strains, we performed ~1 ns NPT (1,000,000 frames) simulations using the Parrinello-Rahman barostat [17] and Andersen thermostat.[8] The stiffness matrix elements were obtained from the appropriate averages, using Eqs. [8] and [9]. A typical matrix, at 100 K using the strain-strain correlation formula is:

$$\begin{bmatrix} \sigma_1 \\ \sigma_2 \\ \sigma_3 \\ \sigma_4 \\ \sigma_5 \\ \sigma_6 \end{bmatrix} = \begin{bmatrix} 6.09 & 3.92 & 3.39 & 0.25 & 0.17 & 0.27 \\ 3.92 & 5.95 & 3.27 & -0.19 & 0.22 & -0.05 \\ 3.39 & 3.27 & 5.64 & -0.11 & 0.00 & -0.07 \\ 0.25 & -0.19 & -0.11 & 1.36 & 0.04 & -0.21 \\ 0.17 & 0.22 & 0.00 & 0.04 & 1.14 & 0.22 \\ 0.27 & -0.05 & -0.07 & -0.21 & 0.22 & 1.25 \end{bmatrix} \begin{bmatrix} \varepsilon_1 \\ \varepsilon_2 \\ \varepsilon_3 \\ \varepsilon_4 \\ \varepsilon_5 \\ \varepsilon_6 \end{bmatrix} \qquad [10]$$

A comparison of the numerical data with the matrix elements expected for an isotropic sample (Eq. [3]) reveals that the results are in good qualitative agreement; e.g. $C_{11} \approx C_{22} \approx C_{33}$, $C_{12} \approx C_{13} \approx C_{23}$, and the remaining elements are significantly lower. One obtains E, B, G and ν via a least-squares fit of the non-zero elements to obtain λ and μ, followed by application of Eqs. [4]-[7].

The temperature dependence of the elastic constants computed from the MD simulations are displayed in Table 2; E, B and G are also plotted in Fig. 2. Values presented represent those obtained from the strain-strain correlation, Eq. [8]. Although not shown, constants from the stress-strain correlation (Eq. [9]) are very close in magnitude. One observes from both table and figure that, all three moduli decrease monotonically with rising temperature. This is expected and reflects softening of the material at higher temperatures. In addition, the MD results for the elastic moduli vary in the order: B > E > G, as is found experimentally for most elastic materials. In addition, as seen from the last column of Table 2, values of the Poisson ratio lie between 0.35 and 0.40, and vary only modestly with temperature. This is common behavior for amorphous polymers well below T_g.

The author is not aware of any mechanical experiments that have been performed on *atactic* polypropylene. In one of the common references commonly quoted for polypropylene mechanical properties in compilations,[19-21] the results are actually for the isotactic stereoisomer.[22] A fairly comprehensive study of the

temperature dependence of tensile moduli of **amorphous** polypropylene has been reported by Sauer, et al.[13] For one of their samples (PP-4 in the reference), they report 0% crystallinity (from IR/X-ray results), but do not indicate the tacticity of the sample. However, to obtain an estimate of the qualitative accuracy of our results, we have extracted values of E(T) [via numerical digitization of data in Fig. 2 of their paper], which are displayed in Table 2 [E(exp)] and plotted in Fig. 2 [open circles]. It was found that the qualitative agreement between E(MD) and E(exp) is fairly good; values from MD are typically 15-30% lower than experiment. The temperature dependence of the computed tensile moduli [$dE(MD)/dT = -9.1$ MPa K^{-1}] is also close the the experimental value [$dE(exp)/dT = -10.4$ MPa K^{-1}]. The level of agreement between calculated and measured moduli is particularly satisfying given uncertainties in the tacticity of the sample, the much greater molecular weight of the experimental specimen [$M_w(exp) \approx 3 \times 10^5$ g mol^{-1} vs. $M_w(MD) \approx 3,200$ g mol^{-1}], and the well-known dependence of measured mechanical properties upon the method of sample preparation and processing history. Theodorou and Suter [14] have also reported the results of an atomistic molecular mechanics simulation of the elastic moduli of aPP. One cannot assign a temperature to the results obtained in that study because, although the model was static (i.e. at 0 K), the amorphous cell was built at a density corresponding to 233 K. Nevertheless, a qualitative of the two sets of results is interesting. As shown in the last row of Table 2, their computed values for E, B and G all lie in the same range as our results between the temperatures of 100 K and 150 K, from which we may conclude that the results of the two investigations are in very reasonable qualitative agreement.

Finally, it is instructive to compare elastic moduli predicted from QSPR with values computed from our MD simulations. These results, determined from Eqs.

[A.6]-[A.8], are plotted in Fig. 2 also plotted in Fig. 2. One may see from the figure that both the magnitudes and temperature dependence of the QSPR agree quite well with values computed from our MD simulations. Specifically, B(QSPR) agrees with B(MD) to within -1% to -21%, with similar levels of agreement for E (-6% to +11%) and G (-4% to +13%).

A.3 Yield Stress of aPP

As discussed in an earlier section, computer experiments were performed in which the the uniaxial stress along a given (x, y, or z) axis in the cell was increased at a constant rate and the resulting strain was measured. This method of studying stress-strain relationships in polymers was first developed by Brown and Clarke,[23] and their or similar methods have been employed successfully in a number of MD investigations of the yield behavior in solid polymers [e.g. Refs. [24-29]]. Displayed in Fig. 3A are the resultant stress vs. strain curves for aPP at three temperatures when the stress was increased at a rate of 5 bar ps^{-1}; similar curves were found for lower rates of stress increase. One observes the general phenomenon in plastic solids that at low stresses, the strain increases linearly with applied "true stress"[30] (elastic behavior). However, at higher stresses, the sample begins to exhibit a very large increase in strain (i.e. catastrohic failure) with little or no further increase in the stress levels.

Because the specific shapes of stress vs. strain curves vary considerably between samples (and even for the same sample at different samples), there are a variety of definitions of the yield stress (σ_y) of a solid,[15] and of the procedures by which σ_y is derived from a specific curve. Qualitatively, though, one may view the yield stress as that value beyond which the plastic solid begins to exhibit liquid-like flow behavior (i.e.the point at which the stress-strain curve approaches a horizontal increase in

12

strain).[31] In order to obtain semi-quantitative estimates of the yield stress (σ_y) and yield strain (ε_y) in our aPP samples, we utilized a common procedure[15] in which tangents were drawn in both the elastic (low ε) and yield (high ε) region of the curves; ε_y and σ_y were determined from the intersection of the two lines. Because the high yield line is close to horizontal, values of σ_y are expected to be more accurate than ε_y (this is true in all graphical procedures used to calculate the yield stress).

Numerical estimates of the yield stress and strain at 3 temperatures and 3 rates of stress increase are contained in Table 3. The values represent the average of two independent runs (using independently built and equilibrated cells), with the mean deviation between runs in parentheses.

As seen clearly in both Fig. 3A and in Table 3, for a given rate of stress increase, the yield stress decreases markedly with increasing temperature. This is expected intuitively, because of the "softening" of the plastic at higher temperature, and has been observed in other MD investigations of yield behavior.[23-29]

One also expects the stress-strain curves and resultant yield stresses to be a function of the rate of stress (or strain) increase on the sample. We have plotted the curves for three rates of stress increase at a given temperature (100 K) in Fig. 3B. Indeed, one finds that the yield stress is lowered as the rate of increase is decreased; this is also found in Table 3 (although the values of σ_y at 200 K are approximately equal for 5 bar ps^{-1} and 3 bar ps^{-1}). Again, this observation is expected on a physical basis because decreased rates of stress increase provide the time required for the polymer segments to reequilibrate in response to increased stress, thus promoting additional yielding of the sample. The same trend has been observed in other MD simulations of polymer stress-strain behavior.[23-29]

To the author's knowledge, the only reported yield stress's of polypropylene have been on the isotactic polymer or on samples of unknown tacticity.[10] Furthermore, it is well known that measured values σ_y on the same polymer can vary markedly and are dependent upon quantities such as molecular weight, sample preparation method and processing history. However, it is still possible to obtain an estimate of the quality of the simulation results by referring to the well-known empirical correlation that the yield stress in a large number of polymeric materials is proportional to the tensile modulus:

$$\sigma_y(T) \approx \kappa \bullet E(t) \qquad [11]$$

with reported values of the empirical proportionality constant constant, κ, ranging from 0.025^{20} to $0.028.^{21}$

Displayed in Fig. 4 are plots of the yield stress in aPP as a function of temperature for each of the three stress rates (5, 3 and 1 bar ps^{-1}). For comparison, a plot of the experimental tensile moduli $(E_{exp})^{13}$ over a similar temerature range is superposed (with the axis for E_{exp} on the right side of the figure).[32] It is very satisfying to note that the slopes of the computed yield stresses are qualitatively quite similar to that of the experimental tensile moduli, indicating that the MD simulations have correctly captured the expected temperature dependence of the yield stresses in aPP.

Quantitatively, we find that the ratios, $\sigma_y(MD) / E_{exp}$, average about 0.050-0.060, which is approximately twice the ratio expected from the empirical correlation found for other polymers (Eq. 11); i.e. the simulated values of σ_y are too high by approximately a factor of two. In actuality, this result is not at all surprising because, by necessity, the rate of stress increase in the simulations are many orders of magnitude greater than those used experimentally. Thus, one expects the computed values of σ_y to be higher

than experiment; this has also been observed in other MD simulations of yield stresses in glassy polymers. [23-29]

Unlike many properties, no accurate semi-quantitative relationships have been developed to predict the dependence of yield stresses on stress (or strain) rate. However, it has been reported that, theoretically, one expects that σ_y should be an increasing linear function of the logarithm of the strain-rate increase (ε_R):[19-21]

$$\sigma_y = \alpha + \beta \cdot \log_{10}(\varepsilon_R) \qquad [12]$$

with $\beta > 0$. As discussed in the computational section, the method used in determining the stress-strain behavior utilizes the rate of increase of the stress (not strain) as an independent variable. However, by assuming an approximately linear plot of stress vs. strain (Fig. 3) up to the yield point $(\varepsilon_y, \sigma_y)$, we can estimate the strain rates (ε_R) from the stress rates (SR) via following relation:

$$\varepsilon_R = \frac{\varepsilon_y \cdot SR \cdot 10^{12}}{\sigma_y} \qquad [13]$$

where the factor 10^{12} converts SR to bar s^{-1}, and the units of ε_R are %•s^{-1}. As noted above, values of ε_y are subject to considerable error. Therefore, in applying Eq. 12, we have used the average value (over the three stress rates) of ε_y. Values of ε_R derived in this manner are given in the last column of Table 3.

Shown in Fig. 5 are plots of σ_y vs. $\log(\varepsilon_R)$ at all three temperatures (100 K, 200 K, 300 K). One can observe from the figure that, to within the scatter generated by inherent uncertainties in determination of σ_y, the yield stresses do increase approximately linearly with logarithm of the strain rate, as predicted by theory.

In summary, we have found that computed yield stresses decrease with rising temperature, and increase at higher strain rates. Both trends are expected intuitively

and observed experimentally. Furthermore, the computed values of σ_y are within a

factor of two of values estimated from an empirical correlation with the tensile modulus,

and exhibit the same temperature dependence as E, as predicted by the correlation.

IVB. Parmax Self-Reinforced Polymers

As noted in the introduction, the structures of the Parmax SRPs and of PPP are

given by:

Ultem-1000   **Parmax-1200**   **Parmax-1500**   **PPP**
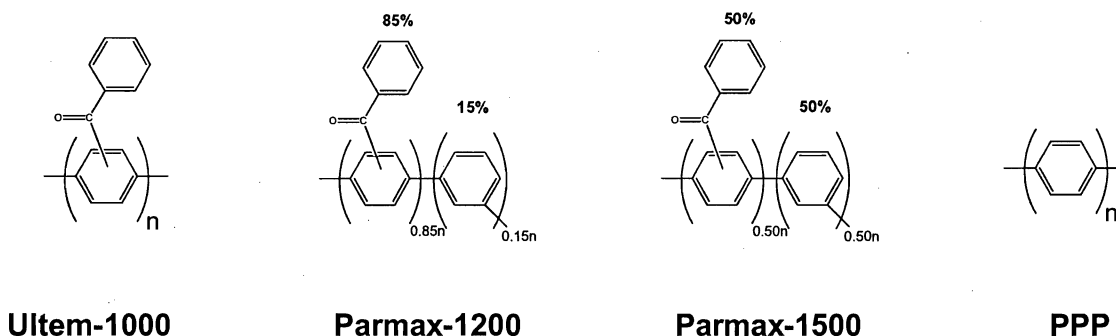
The order of increasing backbone rigidity (i.e. percent of para linkages) is:

Parmax-1500 < Parmax-1200 < Ultem-1000 = PPP. The order of increasing percent of

benzoyl substitution is: PPP < Parmax-1500 < Parmax-1200 < Ultem-1000.

Below, we first discuss volumetric properties [Sect. IVB.1], then mechanical

moduli [Sect. IVB.2] and then yield stresses [Sect. IVB.3]. Where appropriate, results

on the Parmax SRPs are compared with experiments and with trends in molecular

structure.

B.1 Volumetric Properties of Parmax SRPs

From NPT equilibration simulations, values for the cell dimensions were

determined, which yielded densities and, hence, specific volumes ($v_{sp} = 1/\rho$) for each

polymer as a function of temperature. A representative plot of specific volume versus

temperature is given for Parmax-1200 in Fig. 6. The computed specific volume at room

temperature is in reasonable agreement with experiment (within 1.5%) at the one

temperature reported. Values of the glass transition temperature were computed in the standard manner as the intersection of the low and high temperature tangent lines in the specific volume plots. Calculated values of T_g are given in Table 4, together with experimental values for the three Parmax SRPs.[33] It may be seen that the three commercial polymers exhibit very little variation of T_g(exp) with structure (only a total of a 10 K range). One finds too that T_g(MD) is higher than T_g(exp) by 24 to 57 K. This is not surprising and has been found elsewhere. The higher values of T_g(MD) is attributed directly to the much higher rates of sample cooling in the simulations (by many orders of magnitude) than in the experimental measurements.

There is no obvious trend in the computed glass transition temperatures with molecular structure. For example, the two highest values of T_g(MD) are for PPP and Parmax-100, which have the highest and lowest number of para linkages, and thus, the lowest and highest chain flexibility, respectively. Too, the unsubstituted PPP sample exhibits a calculated transition temperature within 6 K of the value for Ultem-1000, which has 100% benzoyl substitution.

B.2 Elastic Moduli of Parmax SRPs

Tabulated in Table 5 and displayed in Fig. 7 are (a) the experimental compressive moduli [in MPa] and (b) experimental compressive strengths [in bar] in the three commercial Parmax SRPs at several temperatures. We note that the compressive modulus should, in principle, be approximately equal the tensile modulus (E), whereas the compressive strength is generally greater than the tensile yield strength (by perhaps 20-50%).[15,19,21]

From Table 5A and Fig. 7A, one finds that the moduli vary in the order: Ultem-1000 < Parmax-1500 < Parmax-1200. One sees the same order in the

17

compressive strengths (Table 5A and Fig. 7B); however, from the figure, the strengths of the three polymers are close to equal at a temperature just below 400 K. This temperature is approximately 30-40 K below T_g in the systems. However, it is not clear why the compressive strengths of three polymers of differing structure should approach each other at the glass transition temperature.

It is of interest that the order of increasing experimental compressive moduli and strengths do not correspond to any apparent trend in structure. For example, the order of increasing molecular backbone rigidity, as indicated by percent para linkages would be Parmax-1500 (50% para) < Parmax-1200 (85% para) < Ultem-1000 (100% para). Note that the trend in increasing benzoyl substitution is the same. Thus, the trend in these structural properties does not correspond to the experimental order of mechanical properties, in which the Parmax-1500 has properties midway between those of Parmax-1200 and Ultem-1000.

We have used the fluctuation strain-strain method [Eq. 8 above] to determine the mechanical Tensile (E), Bulk (B) and Shear (G) moduli + Poisson's ratio (v) in PPP and the three Parmax SRPs. The results are displayed in Table 6 and the moduli are plotted in Fig. 8. As shown in Table 6D, Poisson's ratio (v) generally lies in the range 0.35-0.45 expected for amorphous polymers at temperatures well below T_g.[19,21] Generally, the dependence of v on temperature is very slight (until one reaches close to T_g) and, indeed, the values of this parameter appear to remain approximately independent of T to within scatter in the computed results.

From Table 6 and Fig. 8A, it is clear that the tensile moduli (E) of all four polymers decreases with increasing temperature. This is the same trend observed for aPP (*vide supra*) and expected of the mechanical moduli in amorphous solids.[15,19,21] A

similar decrease in the shear modulus (G) [Fig. 8B] and bulk modulus (B) [Fig. 8C] is observed for all four systems at higher temperatures.

One can see from Tables 6A-6C that, for a given polymer, the mechanical moduli vary in the order: $B(T) > E(T) > G(T)$. As noted in the earlier section on aPP, this is the trend generally found in glassy polymers below the glass transition temperature.

Inspection of Fig. 8A refeals that the calculated tensile moduli vary in the order: $E(Ultem-1000) > E(Parmax-1200) > E(Parmax-1500) > E(PPP)$ at most temperatures. The same order is found for the shear moduli (G) of the four polymers [Fig. 8B]. On the other hand, there is no clear cut trend in computed bulk moduli (B) in the four systems [Fig. 8C]. In retrospect, this is perhaps not surprising because B, as a measure of volume decrease with increasing isotropic compression, is inherently different from E and G,both of which are measures of increased elongational strain upon the application of linear stresses. One also notes that the observed order of decreasing tensile and shear moduli is the same as the trend in decreasing benzoyl substitution: Ultem-1000 [100%] > Parmax-1200 [85%] > Parmax-1500 [50%] > PPP [0%]. While this observation is interesting, it is unfortunate that because the relative backbone rigidities of the polymers (as measured by fractional meta linkage) varies irregularly in the series, one may not conclude that the trend of decreasing mechanical moduli is a direct results of the amount of side-chain substitution.

As noted earlier, it is a reasonable approximation to assume that, for small stresses, the compressive and tensile moduli are close to equal.[15,19,21] Therefore, we can compare our results for the tensile moduli with experimental compressive moduli for the three Parmax SRPs. This is shown in Fig. 9 (experimental data are represented by open symbols).

One first notices that, in general, experimental compressive moduli are significantly greater than computed tensile moduli in Parmax-1200 and Parmax-1500, by factors of 2 to 3, although experimental and calculated values for Ultem-1000 are rather close. One sees, further that among the SRPs, experimental compressive moduli vary in the order: Parmax-1200 > Parmax-1500 > Ultem-1000. Thus, although the the order of predicted moduli from the MD simulations is correct for Parmax-1200 and Parmax-1500, the computed moduli of Ultem-1000 are predicted to be the highest among the SRPs, which is precisely the opposite from the trend found experimentally.

As discussed earlier, the various SRPs differ both in their percent substitution and percent of backbone flexibility. Therefore, it is not possible at this time to ascertain whether the results indicate that there are errors in the predictions for the rigid polymer (Ultem-1000), which lies closest to experiment, or from overestimation of the mechanical moduli for systems with flexible backbones (Parmax-1200 and Parmax-1500). In the last section, we discuss proposed computational experiments to study the effects of benzoyl substitution and backbone rigidity separately.

B.3 Yield Stress of Parmax SRPs

Uniaxial stress experiments (see Sect. III: Computational Procedures) were conducted on the three Parmax SRPs and PPP at temperatures ranging from 50 K to 400 K using a rate of stress increase of 5 bar ps^{-1} in order to determine the stress-strain behavior in these systems. In the earlier section on yield behavior in aPP, it was discussed that values for the yield stress, σ_y were determined from intersection of the linear regions of the curves for low and high stress behavior (see Fig. 3). However, it was found that the stress-strain curves in the Parmax SRPs did not exhibit the same regular behavior; curves for the same polymer at different behaviors and for different

polymers had different shapes. Therefore, we employed an alternative procedures to estimate the yield stress. We measured σ_y as the value of the stress at which the strain reached a constant percent. Of various values used, the most regularly trends were found when values of σ_y were determined as the stress when strain reached 10%.

Values of σ_y estimated in this manner are given in Table 7 for the four systems as a function of temperature; they are also plotted in Fig. 10 (solid symbols). There were some points inconsistent with the surrounding data. These are given in bold italics and the table and are not plotted.

It is satisfying to see from the figure that, in general, the yield stress decreases as the temperature rises. This was found in aPP and is expected because of polymer "softening" as one approaches the glass transition temperature.

One also observes that, although there are exceptions, for a given temperature the yield stresses of the various polymers vary in the order: σ_y(Ultem-1000) > σ_y(Parmax-1200) > σ_y(Parmax-1500) > σ_y(PPP). This precisely the same trend observed for the tensile (and shear) moduli (Fig. 8A) and, as noted above, is the same as the order of decreasing benzoyl substitution.

In the earlier section on yield stress in aPP, it was discussed that there is an empirical linear relationship between yield stresses and tensile moduli in polymeric solids [Eq. (11)]. We have computed values for the ratio, $\kappa = \sigma_y(T)/E(T)$, in the SRPs (being sure to convert the two quantities to the same units). The values of κ range from ~0.05 to 0.09 (with a few values being a bit higher), which is approximately 2-3 times the experimentally observed ratios.[21] However, it is satisfying to note that there is a clear correlation between computed values of these two mechanical properties.

It is of interest to compare calculated yield stresses in the Parmax SRPs with experimental compressive strengths in these systems, keeping in mind that (a) compressive strengths are typically 20-50% higher than yield stresses and (b) we have only rough estimates of σ_y in these systems due to the comparatively irregular behavior of the stress-strain curves. The experimental compressive strengths are also plotted in Fig. 10 (open symbols). One sees that the calculated and measured quantities are in satisfying qualitative agreement with each other. However, it can be seen that, whereas σ_y(Ultem-1000) calculated from MD is highest of the SRPs, this polymer has the lowest compressive strength experimentally. This discrepancy is **precisely** the same that was found when comparing computed tensile and experimental compressive moduli in the last section. Once again, because the percent of benzoyl substitution and backbone rigidity are both varied independently in these systems, it is not possible to ascertain the basis of the deviation between theory and experiment. at this time.

V.   Further Studies

The investigation on the volumetric properties, elastic moduli and yield behavior in atactic polypropylene is close to complete, and the data yield a coherent picture on the mechanical properties of this system. On the other hand, there are many questions which remain about the elastic and yield properties of the Parmax SRPs. A number of studies are planned which can address these issues and yield a better understanding of the capability of MD simulations to model the mechanical behavior in these systems. Specifically, we plan studies of the following type.

1.   **Simulations using independently built cells.** All results reported in this study were obtained by measurements of a single cell of each polymer. When one is computing properties in a polymeric systems containing only 3-4 strands of

22

polymer, then it is possible that the results will differ using different cells with varying structure. The experiments should be repeated with at least one additional cell (and preferably two or more) to see if the computed mechanical properties are cell independent.

2. **Dependence on cell size.** In our earlier studies of fluid properties, we found that cells with lengths of ~25 Å were adequate to replicate macroscopic behavior (using PBCs, of course). However, this may not be true in polymeric solids. Therefore, we will perform selected experiments with larger cells (35-40 Å cell length) to determine whether the results remain the same.

3. **Stress Rate dependence of yield stresses.** It was noted in Sect. IVB.3 that the stress strain curves of the Parmax SRPs yielded irregularly shaped curves, unlike earlier results on aPP. We believe that this may be a result of the commparatively high rate of increase of the applied stress (5 bar ps^{-1}). Therefore, experiments on these systems will be repeated at lower rates of stress increase of 3 and 1 bar ps^{-1} to determine if the stress-strain curves exhibit more regular behavior under the milder conditions.

4. **Comparison with predictions from QSPR.** It was found in our pilot studies on aPP that empirical Quantitative Structure-Property Relations yielded predicted volumetric and mechanical properties that were in reasonably good agreement with those derived from the MD simulations. Because QSPR furnishes a very computationally inexpensive method of property prediction, we will determine if these correlations perform adequately in predicting the various properties in the Parmax SRPs as well.

5. **Conformational Properties.** It is well known that polymer solids distort under stress. We plan to determine conformational properties including end-to-end distances, radii of gyrations, dihedral angle distributions and transition rates, orientational distribution parameters and atomic pair correlation functions in the glassy, rubbery and fluid regimes to monitor changes in these parameters in the varioius phases. In particular, the conformational properties in the glass will be measured under varying stress conditions to determine the correlation between these measures of molecular conformation and the computed mechanical properties. We are particularly interested in comparing dihedral angle distributions and transition rates in the various SRPs to determine the effect of the presumed backbone flexibility (from different percent meta linkages) on these parameters.

6. **Independent variation of backbone flexibility and benzoyl substitution.** In the above discussion of the elastic moduli and stress behavior in the Parmax SRPs, we noted that an unambiguous determination of the effect of structural features on the mechanical properties was not possible because both the fractional substitution and chain flexibilities were varied concurrently in the commercial polymers (undoubtedly as a result of synthetic procedures). With MD simulations, we can vary these structural features independently. For example we will determine the effects of benzoyl substitution on mechanical properties by calculations on PPP polymers (100% para linkages) with varying percentages of benzoyl group substitution. Similarly, experiments on unsubstituted polyphenylenes with varying percents of meta linkages will enable us to determine how the backbone flexibility affects the computed properties.

Experiments of this type will enable us to assess the effects of substitution and flexibility independently.

Appendix: QSPR estimation of polymer properties

The application of Quantitative Structure-Property Relationships (QSPRs) to predict physical properties in polymeric systems has been the subject of much research, (Refs. 19, 20, 21 and references therein) and parameterized semi-empirical equations have been developed which permit the estimation of various volumetric, thermal, mechanical and other properties (e.g. optical, electrical, solution, etc.) with a reasonable degree of accuracy. We have utilized several of these derived equations to predict the values of various properties which have been computed from the MD simulations.

Volumetric Properties

Bicerano[21] has presented a series of equations to predict volumes (specific or molar) in polymers. For systems in which T_g < 298 K, one has the relations:

$$V(T) = 0.15 V(298) \frac{T - T_g}{1.42 T_g + 44.7} + V(298)\left[1 + \alpha_R(298)\left(T_g - 298\right)\right] \quad T < T_g \qquad [\text{A.1}]$$

$$V(T) = V(298)\left[1 + \alpha_R(298)(T - 298)\right] \quad T > T_g \qquad [\text{A.2}]$$

V(298) and α_R(298) are the room temperature volume and thermal expansion coefficient, respectively.

As shown by Seitz,[20] the thermal expansion coefficients in the glass and rubber can be predicted by the relations:

$$\alpha_G(T) = \frac{1}{V_G}\left(\frac{\partial V_G}{\partial T}\right)_P = \frac{1}{T + 9.47 T_g} \qquad [\text{A.3}]$$

$$\alpha_R(T) = \frac{1}{V_R}\left(\frac{\partial V_R}{\partial T}\right)_P = \frac{1}{T + 4.23 T_g} \qquad [\text{A.4}]$$

Elastic Properties

Seitz[20] has developed correlations for the bulk modulus (B) and Poisson's Ratio (ν) in amorphous, glassy polymers (we use the form of the equations presented in Bicerano's book.[21]   The temperature dependence of ν is given by:

$$\nu(T) = \nu_0 + \frac{50\,T}{T_g}\left\{0.000163 + \exp\left[0.459\left(T - T_g - 13\right)\right]\right\}$$

[A.5]

ν_0 is the Poisson's ratio at T = 0 K, and can be determined if one has an experimental (or estimated) value of $\nu(T)$ at some higher temperature.

The temperature dependence of the bulk modulus can be predicted from the expression:[20,21]

$$B(T) = 8.2333\,E_{coh1}\left[\frac{5V_{mol}(0)^4}{V_{mol}(T)^5} - \frac{3V_{mol}(0)^2}{V_{mol}(T)^3}\right]$$

[A.6]

In this equation, $V_{mol}(0)$ and $V_{mol}(T)$ are the molar volumes at T = 0 K and the temperature of interest, and $E_{coh\,1}$ is the Fedors estimate (via group contributions) of the cohesive energy.[34]   As written, if V_{mol} and $E_{coh\,1}$ are given in $cm^3\ mol^{-1}$ and $J\ mol^{-1}$, respectively, then the units on B(T) are MPa.

In amorphous glassy solids, there are only two independent elastic constants. Therefore, if $\nu(T)$ and B(T) are known experiment or, in this case, estimated from Eqs. [A.5] and [A.6], the tensile and shear moduli (E and G) can be obtained from the relations:[15,35]

$$E(T) = 3B(T)[1 - 2\nu(T)]$$ [A.7]

and

$$G(T) = \frac{3}{2} \frac{1 - 2\nu(T)}{1 + \nu(T)} B(T)$$ [A.8]

It should be noted that the dependence of Poisson's ratio on temperature is very modest until one approaches temperatures close to T_g (e.g. $T \geq T_g - 20$ K). Therefore, from Eqs. [A.7] and [A.8], one expects an approximately constant proportionality between the three moduli, B, E and G.

Yield Stress

There have been several correlations developed between the ultimate strength of a glassy polymer, as measured by the yield stress (σ_y) and the elastic moduli. It has been found that, at low strain rates, there is a direct proportionality between $\sigma_y(T)$ and $E(T)$:[20,21]

$$\sigma_y(T) = \kappa \cdot E(T)$$ [A.9]

Two commonly used values of the proportionality constant are $\kappa = 0.25$ (Ref. 20) or $\kappa = 0.28$ (Ref. 21).

It has also been found that when the rate of strain increase on a polymeric solid is increased, the yield stress rises. A very approximate proportionality is given by:[21]

$$\sigma_y(T) = \kappa \cdot E(T) + \beta \frac{T}{V_s} \ln\left[\frac{\dot{\varepsilon}}{\dot{\varepsilon}_0}\right]$$

where V_s and $\dot{\varepsilon}$ are empirical constants. Thus, one expects a proportionality between

σ_y and $\ln(\dot{\varepsilon})$ at high strain rates.

REFERENCES

1   Mississippi Polymer Technologies, Inc.

2   Accelrys Inc., 9685 Scranton Rd., San Diego, CA 92121-3752

3   H. Sun and D. Rigby, Spectrochim. Acta, Part A **53**, 1301 (1997).

4   D. Rigby, H. Sun, and B. E. Eichinger, Polymer Intl. **44**, 311 (1997).

5   H. Sun, J. Phys. Chem. B. **102**, 7338 (1998).

6   D. Rigby, Fluid Phase Equilibria **217**, 77 (2004).

7   Accelrys Inc., 9685 Scranton Rd., San Diego, CA 92121-3752

8   H. C. Andersen, J. Chem. Phys. **72**, 2384 (1980).

9   H. J. C. Berendsen, P. M. Postma, W. F. van Gunsteren, A. DiNola, and J. R. Haak, J. Chem. Phys. **81**, 3684 (1984).

10   S. C. Sharma, L. Mandelkern, and F. C. Stehling, Polymer Letters **10**, 345 (1972).

11   A. Eckstein, J. Suhm, C. Friedrich, R. D. Maier, J. Sassmannshausen, M. Bochmann, and R. Mülhaupt, Macromolecules **31**, 1335 (1998).

12   D. Kilburn, D. Bamford, G. Dlubek, J. Pionteck, and M. A. Alam, J. Polym. Sci. B **41**, 3089 (2003).

13   J. A. Sauer, R. A. Wall, N. Fuschillo, and A. E. Woodward, J. Appl. Phys. **29**, 1385 (1958).

14   D. N. Theodorou and U. W. Suter, Macromolecules **19**, 139 (1986).

15   I. M. Ward and J. Sweeney, *An Introduction to the Mechanical Properties of Solid Polymers*, 2nd. ed. (John Wiley and Sons, Chichester, England, 2004).

16   E. Riande, *Polymer Viscoelasticity.* (Marcel Dekker, New York, 2000).

17   M. Parrinello and A. Rahman, J. Chem. Phys. **76**, 2662 (1982).

18   A. A. Gusev, M. M. Zehnder, and U. W. Suter, Phys. Rev. B **54**, 1 (1996).

19   D. W. van Krevelen, *Properties of Polymers: Their Correlation with Chemical Structure*, 3rd. ed. (Elsevier, Amsterdam, 1990).

20   J. T. Seitz, J. Appl. Polym. Sci. **49**, 1331 (1993).

21   J. Bicerano, *Prediction of Polymer Properties*, 3rd. ed. (Marcel Dekker, Inc., New York, 2002).

22   R. W. Warfield and F. R. Barnet, Angew. Makromol. Chem. **27**, 215 (1972).

23   D. Brown and J. H. R. Clarke, Macromolecules **24**, 2075 (1991).

24   S. S. Jang and W. H. Jo, Macromol. Theory Simul. **8**, 1 (1999).

25   S. S. Jang and W. H. Jo, J. Chem. Phys. **110**, 7524 (1999).

26   S. S. Jang and W. H. Jo, Polymer **40**, 919 (1999).

27   F. M. Capaldi, M. C. Boyce, and G. C. Rutledge, Phys. Rev. Letters, 175505 (2002).

28   F. M. Capaldi, M. C. Boyce, and G. C. Rutledge, Polymer **45**, 1391 (2004).

29   A. V. Lyulin, N. K. Balabaev, M. A. Mazo, and M. A. J. Michels, Macromolecules **37**, 8785 (2004).

30   The stresses presented here represent the "true stress", which is the applied uniaxial force divided by the actual cross sectional area of the sample at each point, which is lower than the nominal area prior to application of the stress.

31   A. G. Marangoni and M. A. Rogers, Appl. Phys. Letters **82**, 3239 (2003).

32   To facilitate the comparison, experimental tensile moduli plotted in Fig. 4 were converted from MPa (Table 2) to bar.

33   D. Dean, M. Husband, and M. Trimmer, J. Polym. Sci. B **70**, 2971 (1998).

34   R. F. Fedors, Polym. Eng. Sci. **14**, 147 (1974).

35   J. R. Fried, *Polymer Science and Technology*, 2nd. ed. (Prentice Hall, Upper Saddle River, N. J., 2003).

Table 1. Volumetric Properties of aPP.

A. Specific Volumes

T [K]	V_{sp}[exp] [$cm^3 g^{-1}$]	V_{sp}[(A)[a]] [$cm^3 g^{-1}$]	V_{sp}[QSPR] [$cm^3 g^{-1}$]
50		1.092	1.068
100		1.108	1.088
150		1.125	1.108
200		1.141	1.129
250		1.163	1.149
298	1.17[b]		
300	1.175[c]	1.184	1.178
350	1.213[c]	1.216	1.218
400	1.256[c]	1.264	1.258
450		1.301	1.298
463	1.31[d]		
500		1.346	1.338

Table 1. (Cont'd.)

B. Thermal Expansion Coefficients
and Glass Transition Temperatures

Quantity	Exp.	MD[xe]	QSPR
$10^4\,\alpha_G$ [K^{-1}]	1.9[a]	2.81	3.67
	2.7[f]	(0.13)	[3.66][h]
	3.9[g]		
$10^4\,\alpha_R$ [K^{-1}]	6.9[b]	6.53	6.26
	7.1[d]	(0.13)	[6.30][i]
	7.2[g]		
T_g [K]	250[g]	293	277
	275[b]	(4)	
	277[d]		

Footnotes

a) Values from one of two MD runs.

b) Ref. 12.

c) Ref. 13. Numerical values computed from numerical digitization of data in Fig. 3 of reference.

d) Ref. 11.

e) Results are the average of two simulations. values in parentheses are the mean deviation from the avera

f) Refs. 14.

g) Ref. 10.

i) Calculated at 125 K from Eq. [A.3]. Assumed T_g = 275 K.

i) Calculated at 425 K from Eq. [A.4]. Assumed T_g = 275 K.

Table 2. Elastic Moduli of aPP.

T [K]	E(exp)[a] [MPa]	E(MD)[b] [MPa]	B(MD)[b] [MPa]	G(MD)[b] [MPa]	ν(MD)[b]
100	3870	3350 (100)	4320 (10)	1220 (40)	0.37 (<0.01)
150	3510	2540 (230)	3340 (10)	920 (90)	0.38 (<0.01)
200	3040	2310 (300)	2880 (220)	850 (120)	0.37 (0.01)
250	2510	1700 (260)	2180 (10)	620 (110)	0.39 (0.02)
--[c]		2890	3320	1065	0.36

Footnotes

a) Ref. 13. Values obtained by numerical digitization of data in Fig. 3 of reference.

b) Values represent average of the two simulations, using the Strain-Strain correlation equation (Eq. [8]).

c) Ref. 14. Moduli were calculated in absence of kinetic energy (i.e. at 0 K), but using cells built to the experimental density at 233 K.
   Moduli represent the average value obtained from two methods in Table 1 of the reference.

Table 3. Temperature and Stress Rate Dependence of Yield Stress (σ_y) and Yield Strain (ε_y) in aPP.[a]

T [K]	Stress Rate [bar ps^{-1}]	σ_y [bar]	ε_y [%]	ε_R [% s-1]
100	5	2340 (3)	7.6 (0.8)	1.62E+10
	3	2100 (70)	7.7 (0.3)	1.10E+10
	1	2030 (10)	7.3 (0.6)	3.61E+09
200	5	1770 (40)	9.2 (0.1)	2.61E+10
	3	1800 (30)	10.6 (1.8)	1.77E+10
	1	1390 (80)	8.9 (2.5)	6.41E+09
300	5	1400 (30)	9.8 (0.6)	3.49E+10
	3	1300 (20)	9.4 (3.2)	2.16E+10
	1	990 (10)	7.4 (0.8)	7.45E+09

a) Values represent the average of two simulations.
   Quantities in parentheses are the mean deviation from the average.

Table 4. Experimental and Computed Glass Transition
Temperatures in Parmax SRPs.

Species	T_g(exp) [K]	T_g(MD) [K]
PPP	--	483
Ultem-1000	438	489
Parmax-1200	433	457
Parmax-1500	443	500

a) Ref. 33.

b) Mississippi Polymer Technologies, Inc.
Data provided to AFRL/ML.

Table 5. Experimental Mechanical Properties of Parmax SRPs.[a]

A. Compressive Modulus

T	Ultem-1000	Parmax-1200	Parmax-1500
[K]	[MPa]	[MPa]	[MPa]
219	4620	9500	7720
298	3790	8840	6810
394	3190	6590	5500

B. Compressive Strength

T	Ultem-1000	Parmax-1200	Parmax-1500
[K]	[bar]	[bar]	[bar]
219	1860	2730	2510
298	1520	2240	1900
394	980	1050	1030

a) Missippii Polymer Technologies, Inc.
   Data provided to AFRL/ML

Table 6. Computed Elastic Constants of Parmax SRPs.[a]

A. Tensile Modulus (E)

T [K]	PPP [MPa]	Ultem-1000 [MPa]	Parmax-1200 [MPa]	Parmax-1500 [MPa]
100	2438	4427	3277	3458
200	1742	3799	**4348**	2657
300	1162	2777	2348	1907
400	652	2558	2412	1101

B. Bulk Modulus (B)

T [K]	PPP [MPa]	Ultem-1000 [MPa]	Parmax-1200 [MPa]	Parmax-1500 [MPa]
100	7693	5366	6255	5127
200	5455	4996	5284	4873
300	3887	2956	4234	4273
400	1995	3290	3048	2992

Table 6. (Cont'd.)

C. Shear Modulus (G)

T [K]	PPP [MPa]	Ultem-1000 [MPa]	Parmax-1200 [MPa]	Parmax-1500 [MPa]
100	842	1624	1160	1246
200	602	1383	1595	943
300	401	1034	834	669
400	226	933	882	383

D. Poisson's Ratio (ν)

T [K]	PPP	Ultem-1000	Parmax-1200	Parmax-1500
100	0.447	0.363	0.413	0.388
200	0.447	0.373	0.363	0.409
300	0.450	0.343	0.408	0.426
400	0.446	0.370	0.368	0.439

a) Computed using the strain-strain correlation (Eq. 8).

Table 7. Calculated Yield Stress at 10% Strain in Parmax SRPs.[a,b]

T	PPP	Ultem-1000	Parmax-1200	Parmax-1500
[K]	[bar]	[bar]	[bar]	[bar]
50	1770	*1898*	2868	1796
100	1385	2604	2780	1472
150	1219	--	--	*2196*
200	1160	2348	--	1563
250	--	2318	2127	1440
300	1038	*1918*	1809	1155
350	1095	2129	*1264*	*1457*
400	760	1910	1763	1104

a) Entries with a "--" indicate that the run "crashed" before the strain reached 10

b) Entries in **bold italics** are inconsistent with surrounding data. These points were not plotted in the figure.

Figure Captions

1. Specific Volume of aPP.

   ● - Calculated from MD simulation [A represents one of two runs]
   ◇ - Ref. R2 (Eck)
   □ - Ref. R5 (Sauer)
   △ - Ref. R3 (Dlubek)
   ----- - Calculated from QSPR.

   ······ - Tangents to MD volumes in glass and rubber regions [lines have been displaced downward by 0.04 cm^3 g^{-1} for clarity].

2. Elastic Moduli of aPP.
   ■ - B(MD); Bulk modulus computed from MD simulation.
   ◆ - G(MD); Shear modulus computed from MD simulation.
   ● - E(MD); Tensile modulus computed from MD simulation.
   ○ - E(exp); Experimental tensile modulus; Ref. 13

   —— - B(QSPR); Bulk modulus from QSPR.

   ······ - G(QSPR); Shear modulus from QSPR.
   ----- - E(QSPR); Tensile modulus from QSPR.

3. Stress vs. Strain Curves in aPP.

   A. Dependence on Temperature (Stress Rate = 5 bar ps^{-1}).
   B. Dependence on Stress Rate (T = 100 K).

4. Temperature Dependence of Yield Stress in aPP.

   ○ —— - σ_y (SR = 5 bar ps^{-1})
   □ ----- - σ_y (SR = 3 bar ps^{-1})
   ◇ ······ - σ_y (SR = 1 bar ps^{-1})
   ● -·-·- - E(exp)

5. Dependence of Yield Stress on log(Strain Rate) in aPP

   ● —— - T = 100 K
   ■ ----- - T = 200 K
   ◆ ······ - T = 300 K
   The lines through the points were drawn qualitatively.

6. Specific Volume of Parmax-1200.

   ● - Calculated from MD simulation
   ○ - Experimental (Bars represent error limits)

   ······ - Tangents to MD volumes in glass and rubber

7. Experimental Mechanical Properties of Parmax SRPs
   (A) Experimental Compressive Moduli
   (B) Experimental Compressive Strengths

   ● - Ultem-1000
   ■ - Parmax-1200
   ◆ - Parmax-1500

8. Calculated Mechanical Properties of Parmax SRPs
   (A) Calculated Tensile Moduli
   (B) Calculated Shear Moduli
   (C) Calculated Bulk Moduli

   ▲ ‒‒‒ - PPP [MD]
   ●----- - Ultem-1000 [MD]

   ■······ - Parmax-1200 [MD]
   ◆-·-·- - Parmax-1500 [MD]

9. Comparison of Calculated and Experimental Moduli in Parmax SRPs

   ●----- - Ultem-1000 [MD]

   ■······ - Parmax-1200 [MD]
   ◆-·-·- - Parmax-1500 [MD]
   ○ - Ultem-1000 [exp]
   □ - Parmax-1200 [exp]
   ◇ - Parmax-1500 [exp]

10. Calculated Yield Stresses (at 10% Strain) of Parmax SRPs

    ▲ ‒‒‒ - PPP [MD]
    ●----- - Ultem-1000 [MD]

    ■······ - Parmax-1200 [MD]
    ◆-·-·- - Parmax-1500 [MD]
    ○ - Ultem-1000 [exp]
    □ - Parmax-1200 [exp]
    ◇ - Parmax-1500 [exp]

Fig. 1: Specific Volume of aPP
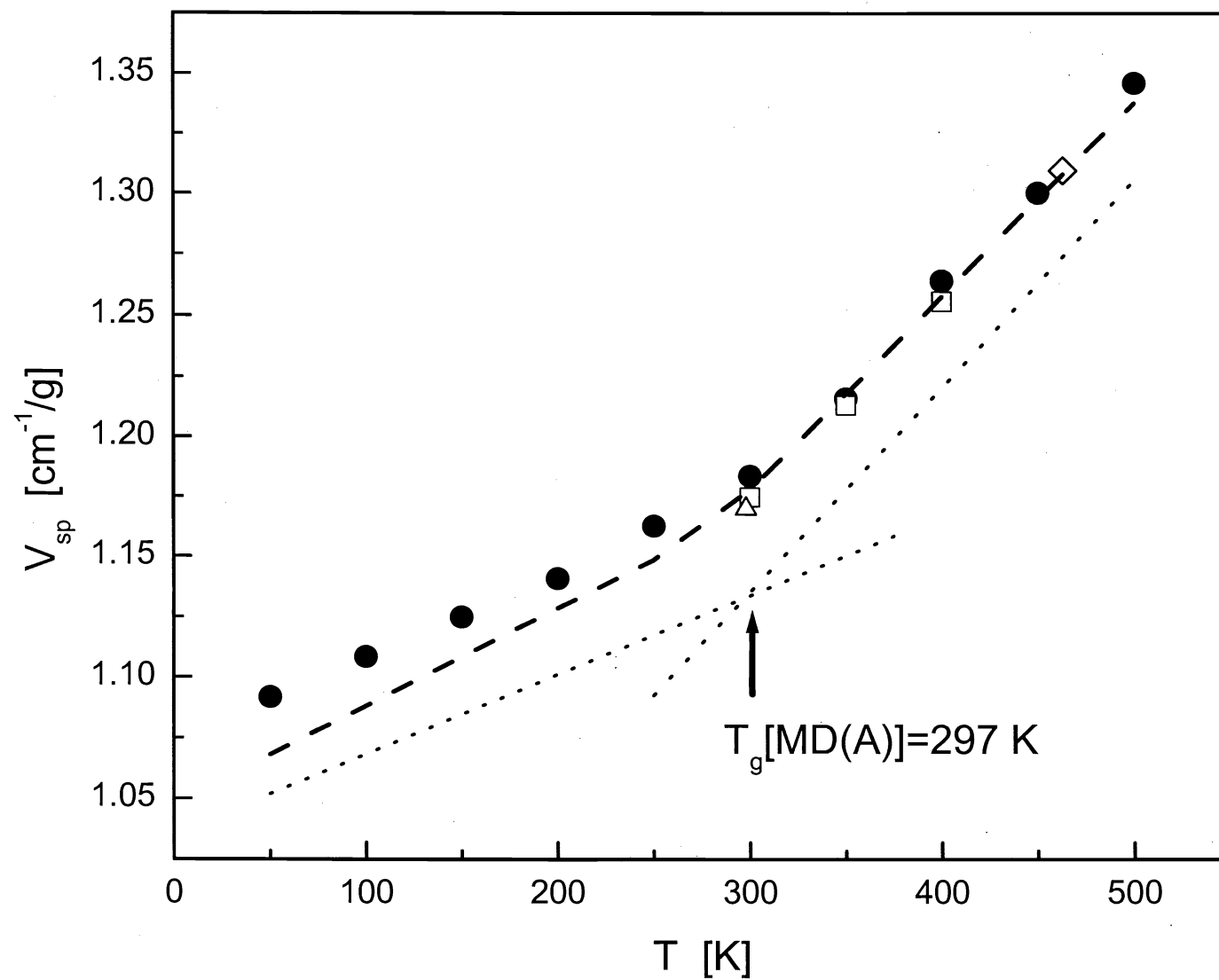
Fig. 2: Elastic Moduli of aPP
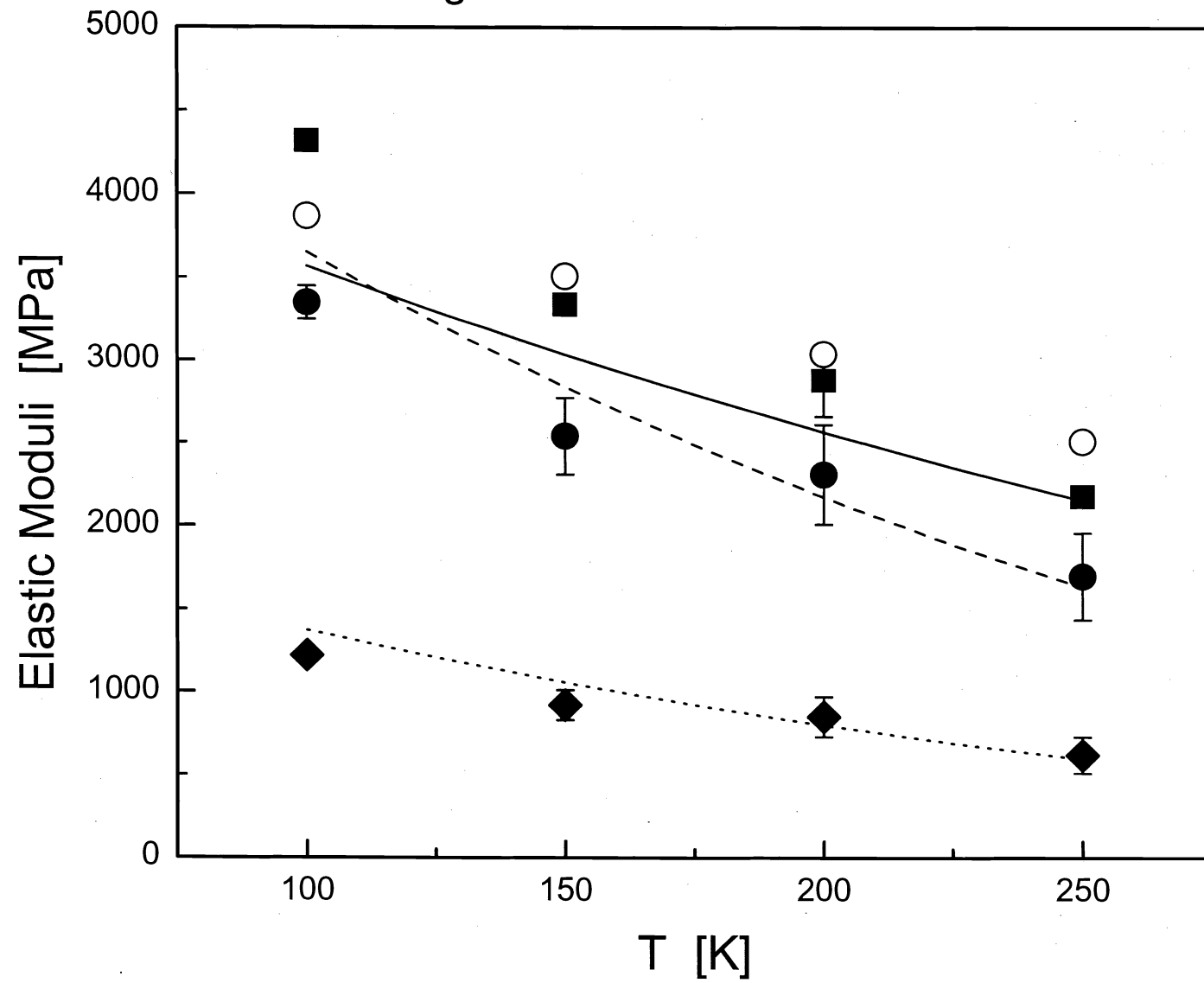
Fig. 3A: Stress vs. Strain Curve in aPP
Dependence on Temperature

T = 100 K

T = 200 K

T = 300 K

Stress [bar]
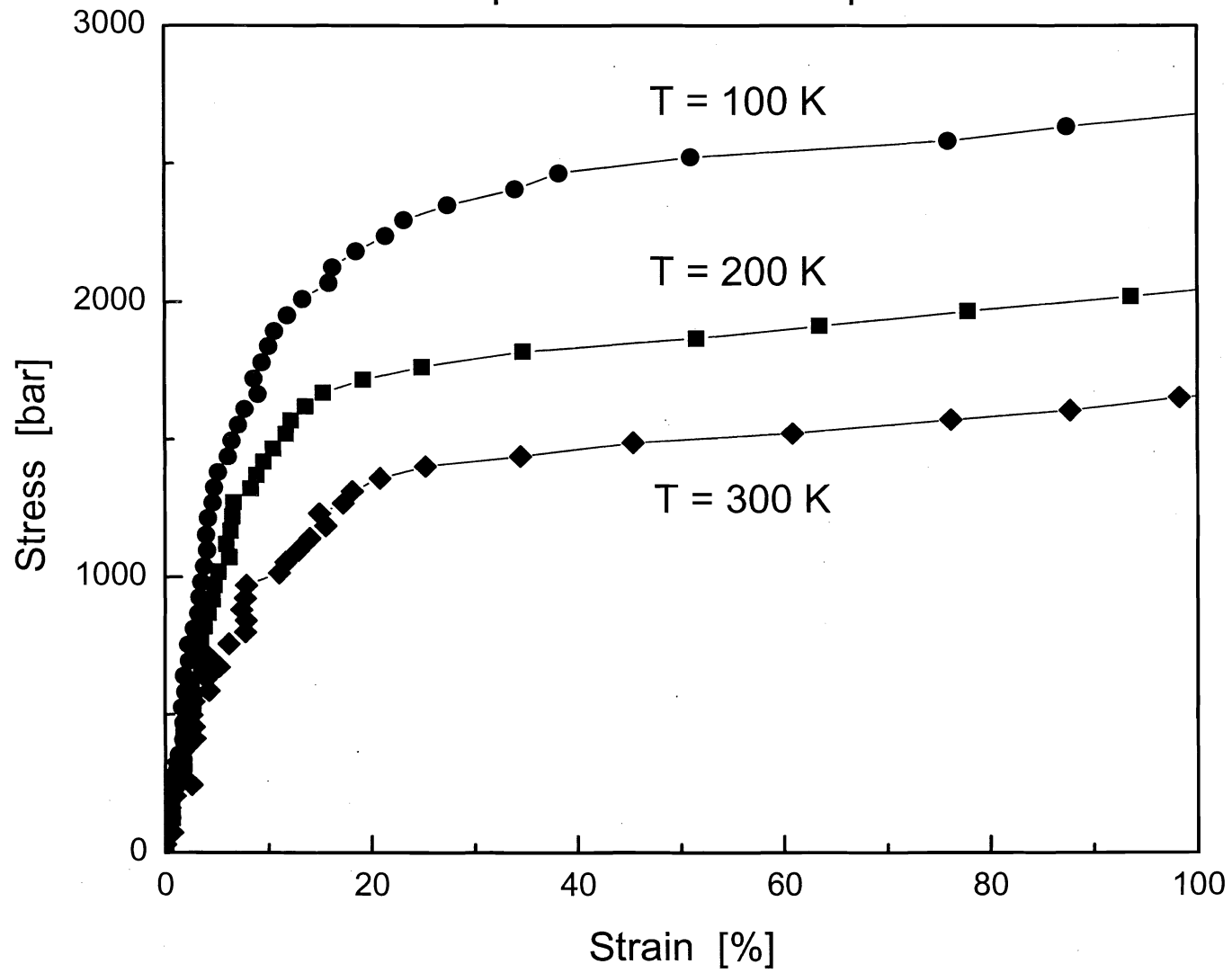
Strain [%]

Fig. 3B: Stress vs. Strain Curve in aPP
Dependence on Stress Rate
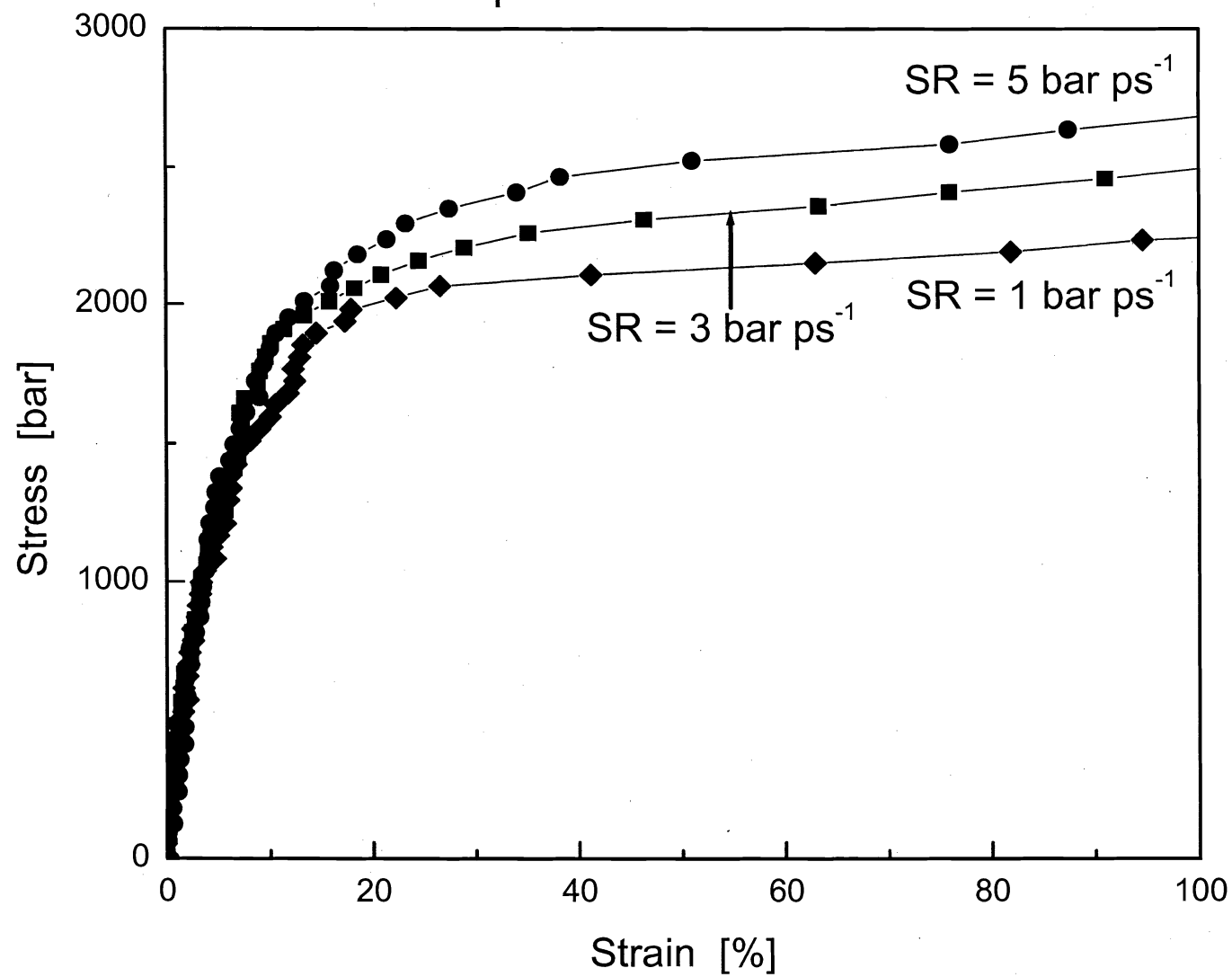
Fig. 4: Temperature Dependence of Yield Stress
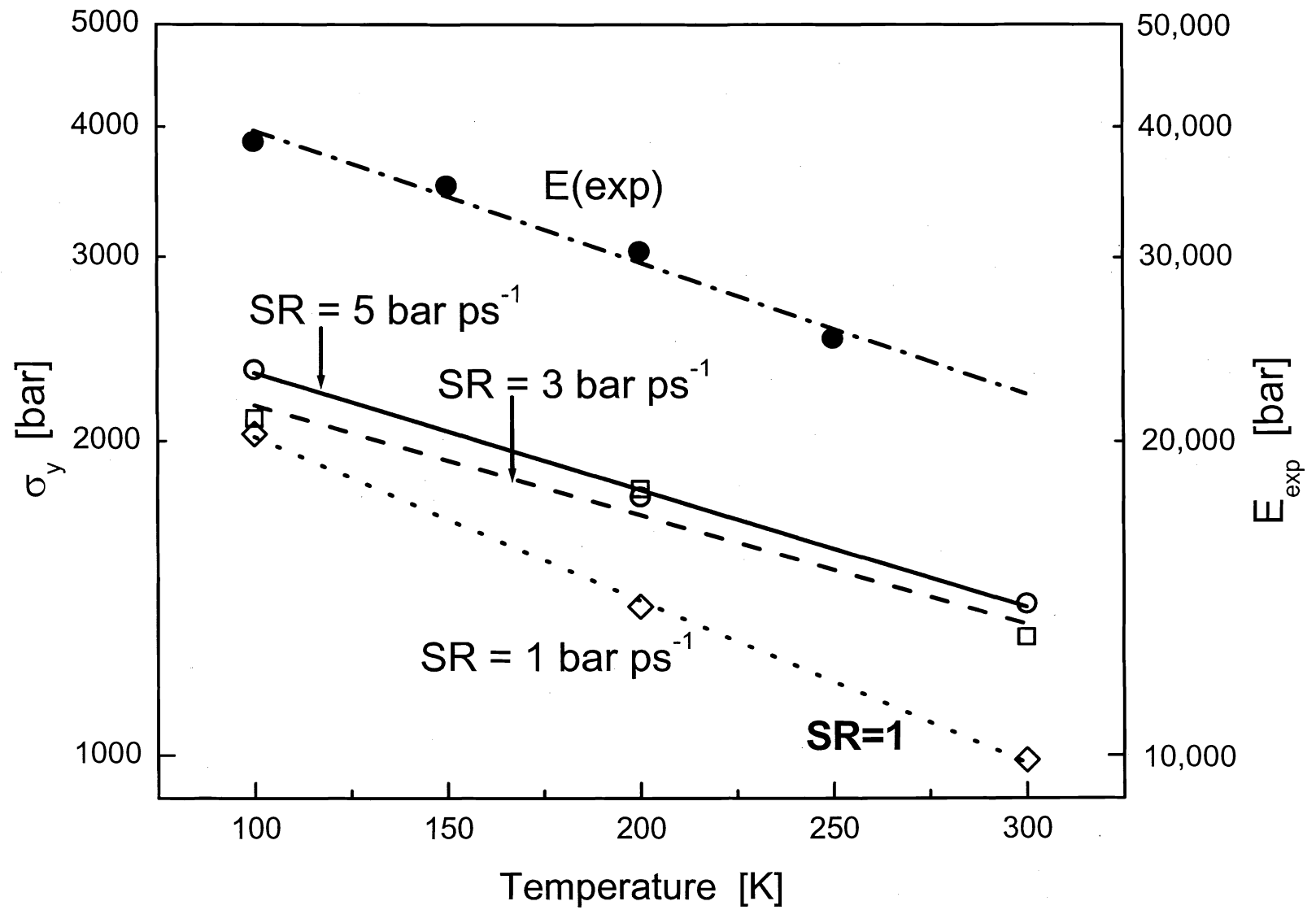
Fig. 5: Dependence of Yield Stress on log(strain rate) in aPP

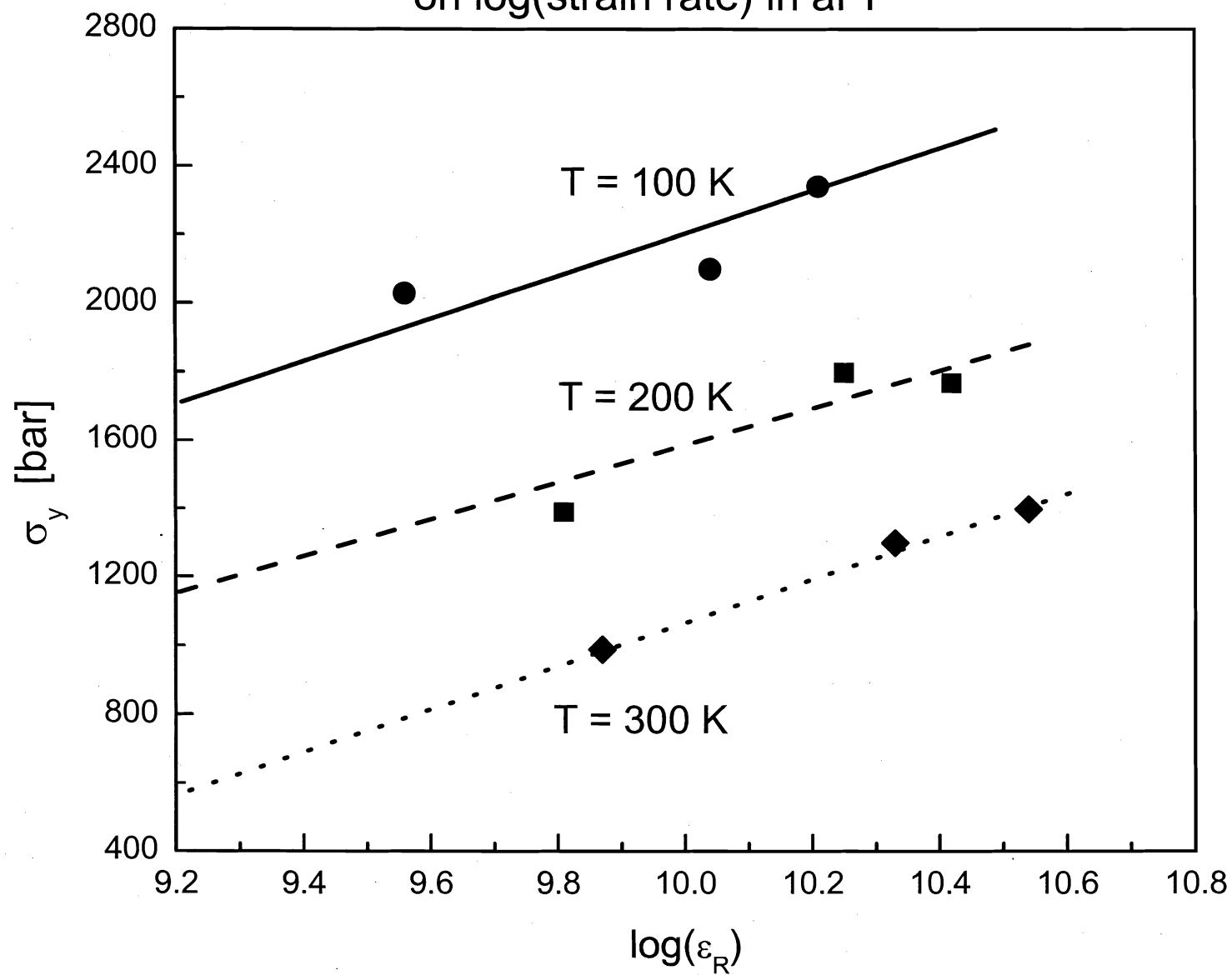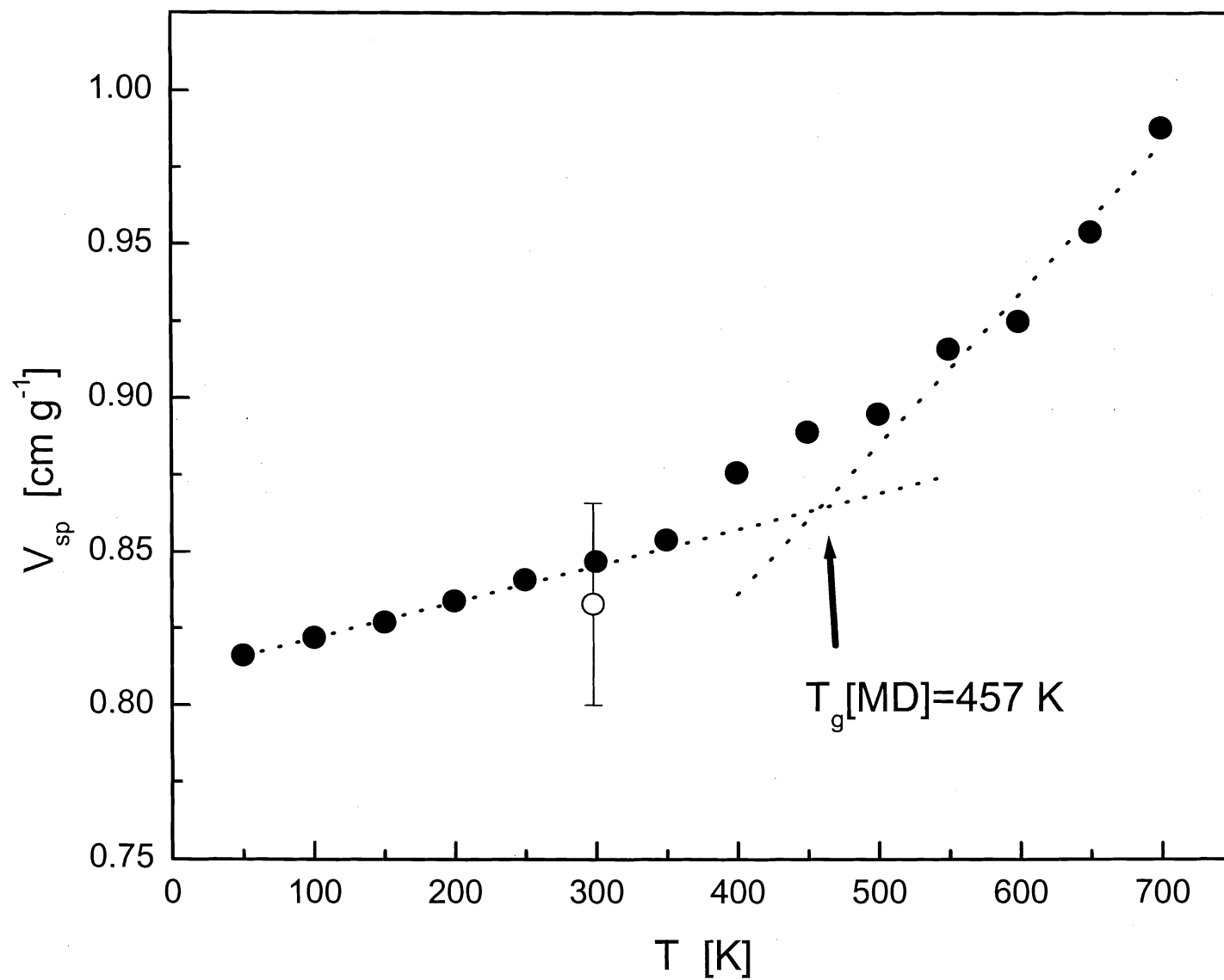Fig. 6: Specific Volume of Parmax-1200

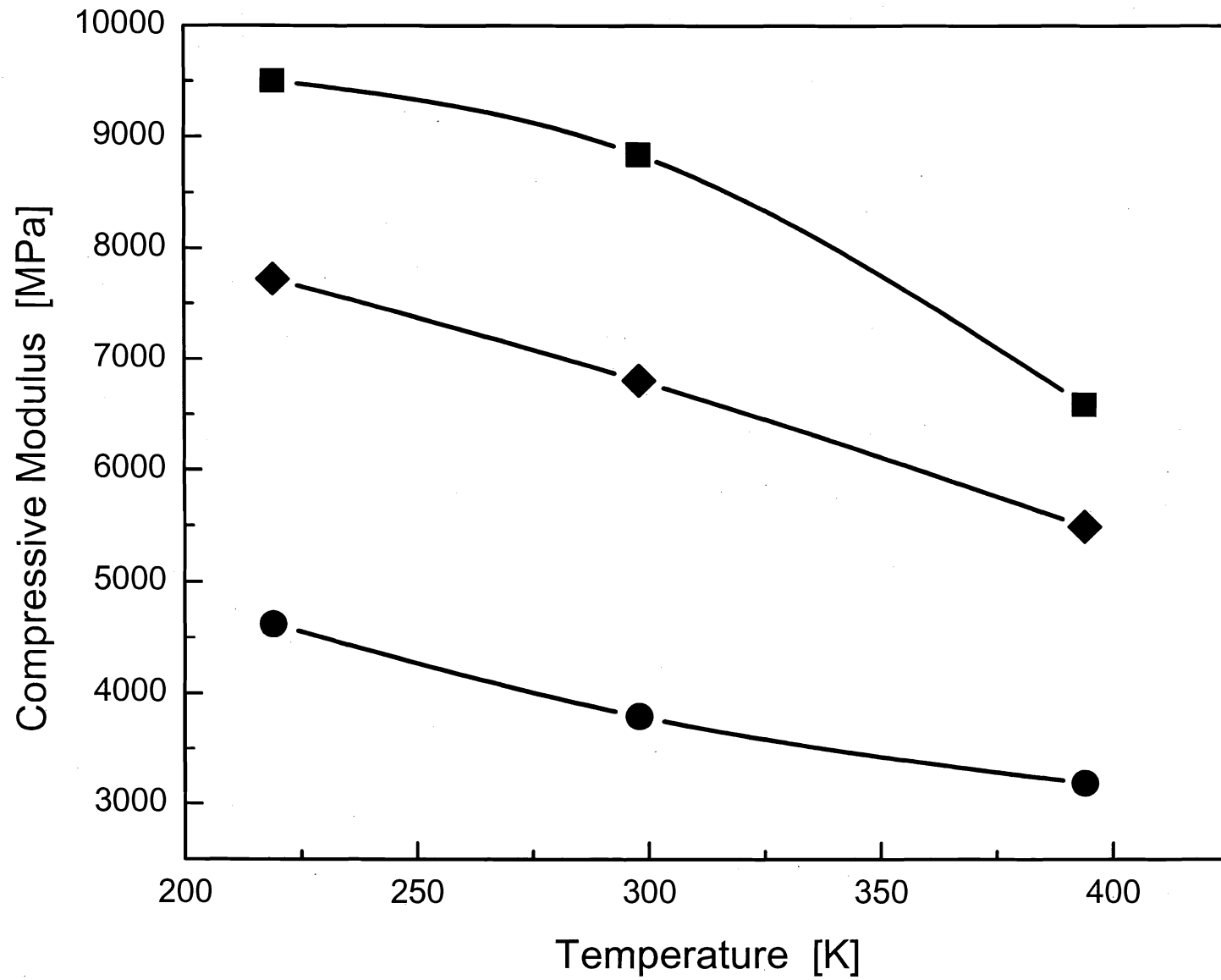T_g[MD]=457 K

Fig. 7A: Exptl. Compressive Modulus of Parmax SRPs

Fig. 7B: Exptl. Compressive Strength of Parmax SRPs
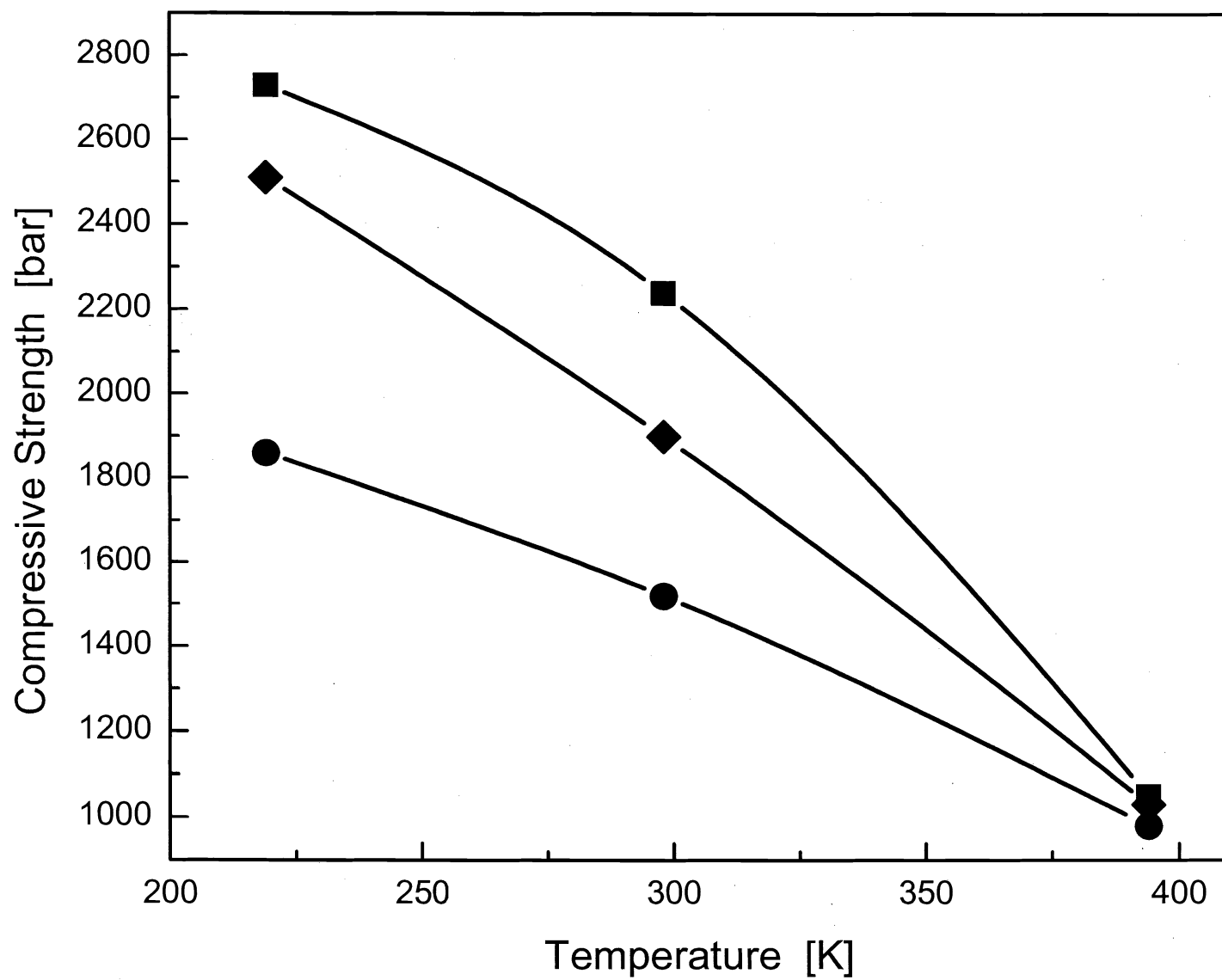
Fig. 8A: Calc'd. Tensile Moduli of Parmax SRPs
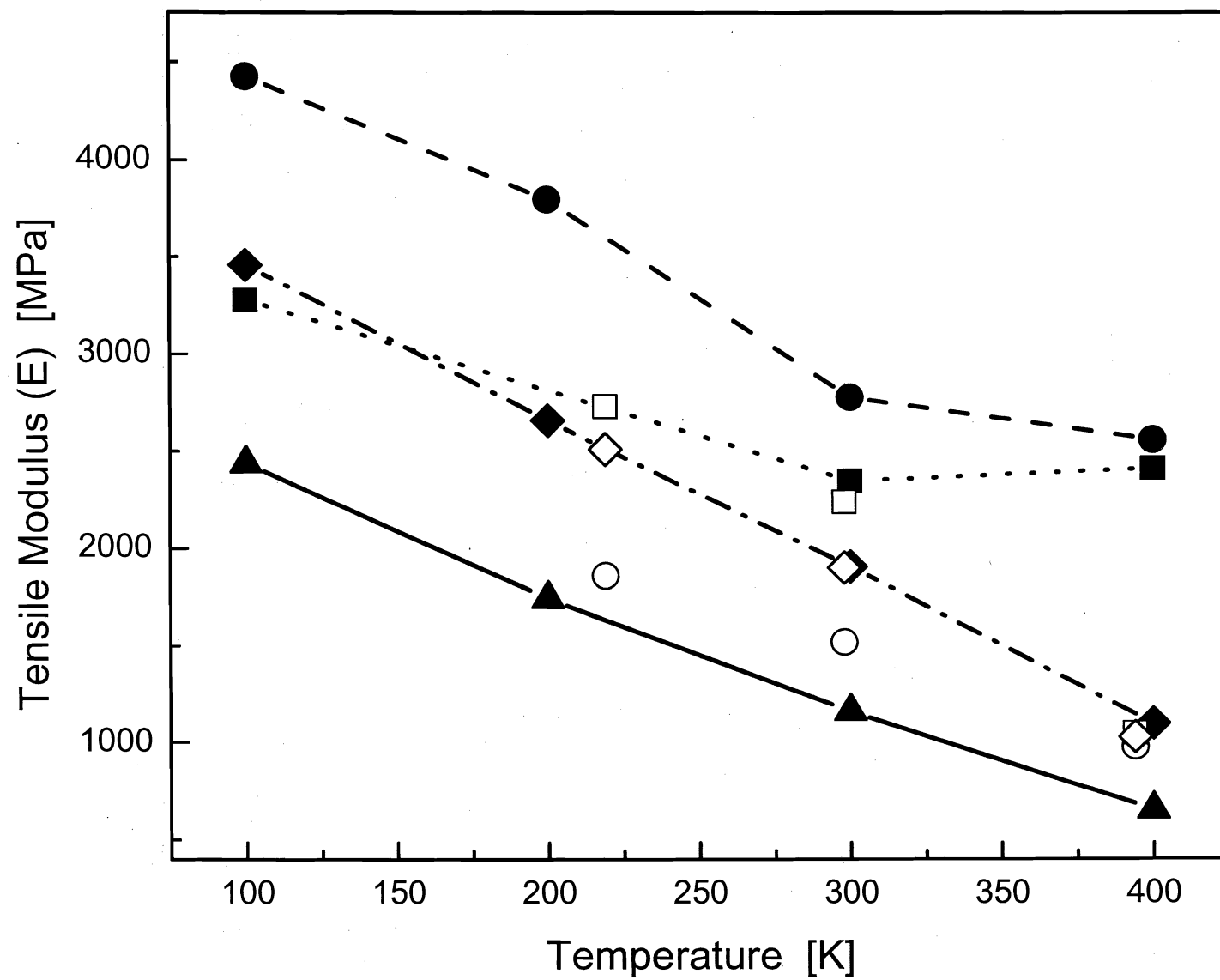
Fig. 8B: Calc'd. Shear Moduli of Parmax SRPs
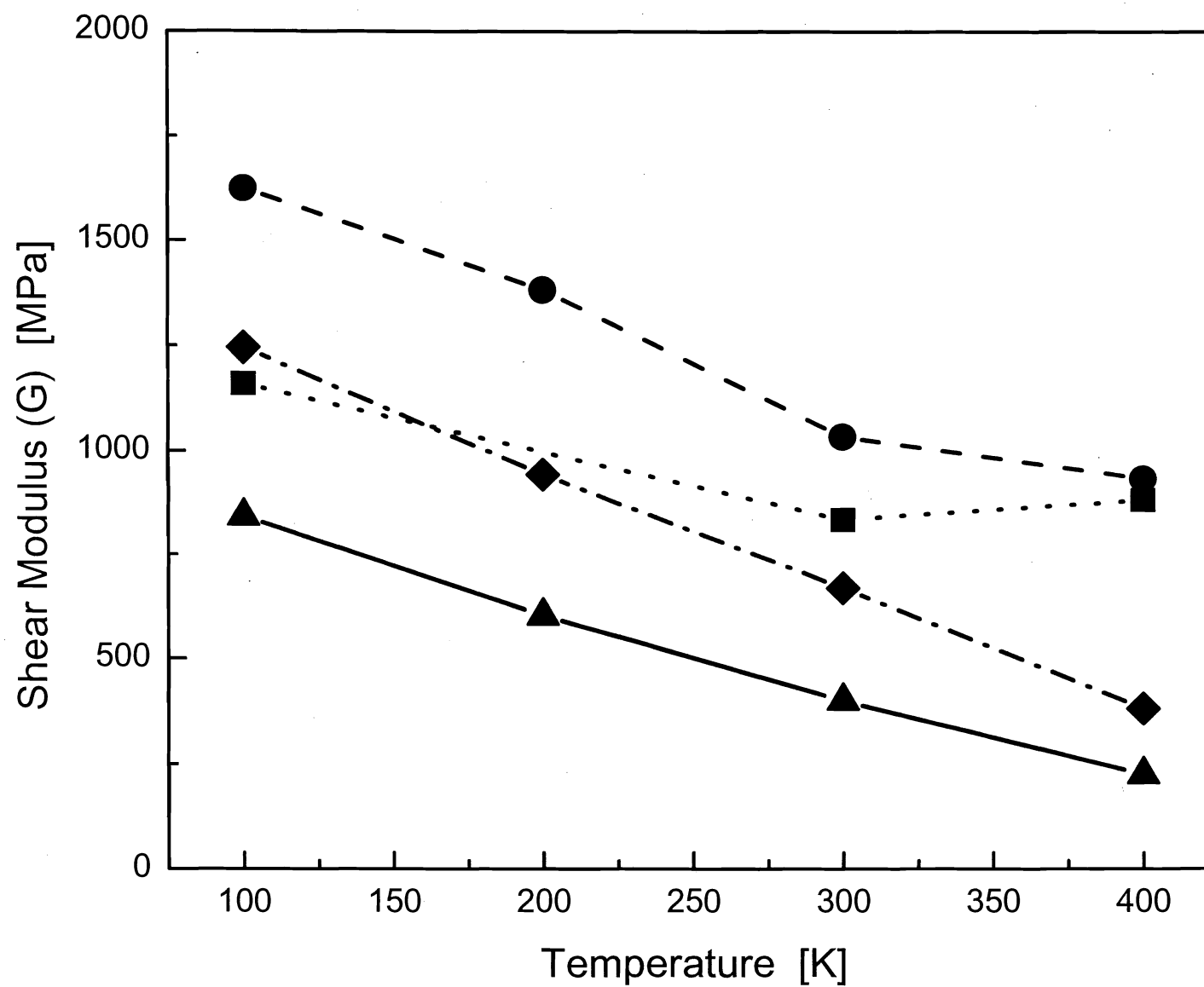
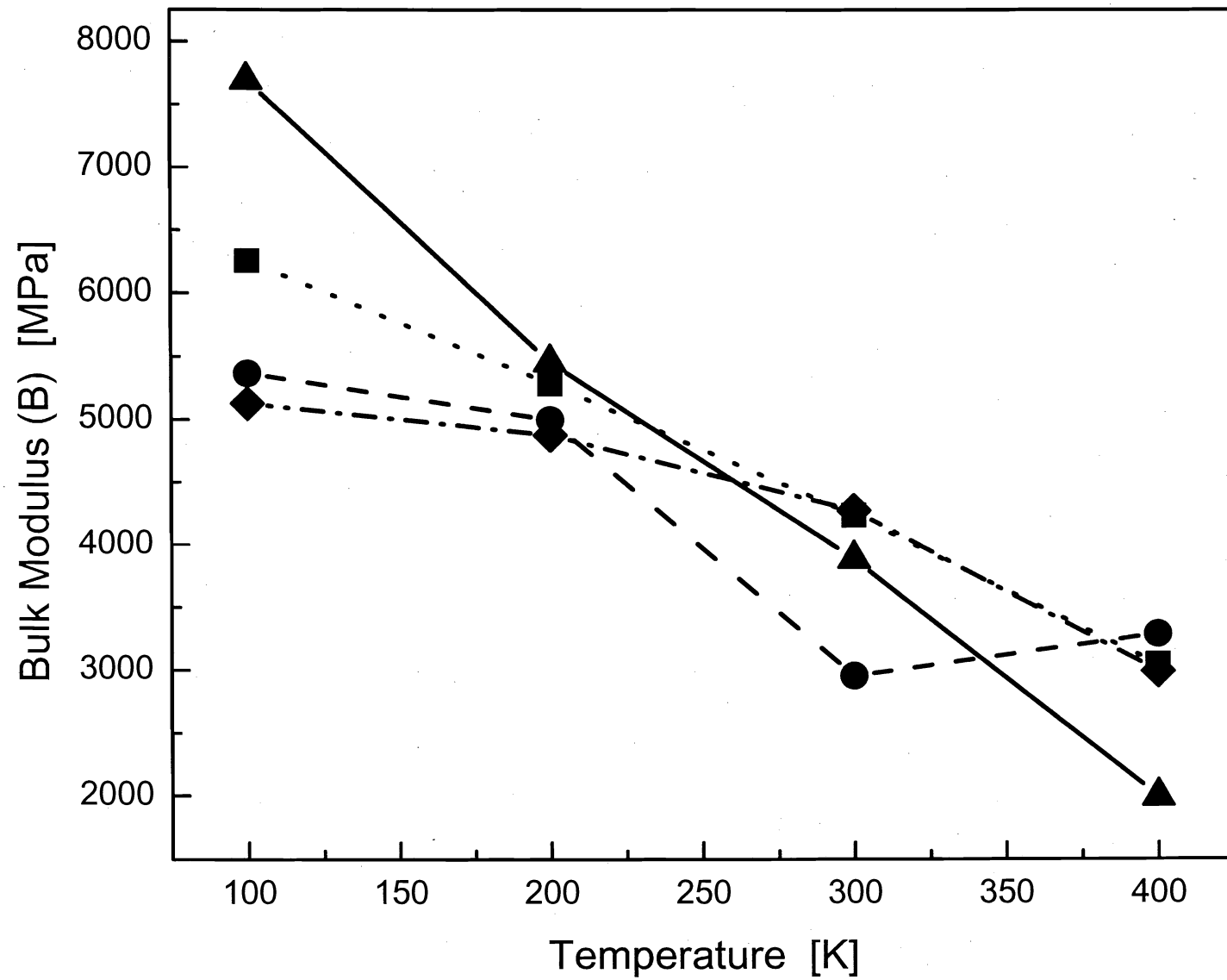Fig. 8C: Calc'd. Bulk Moduli of Parmax SRPs

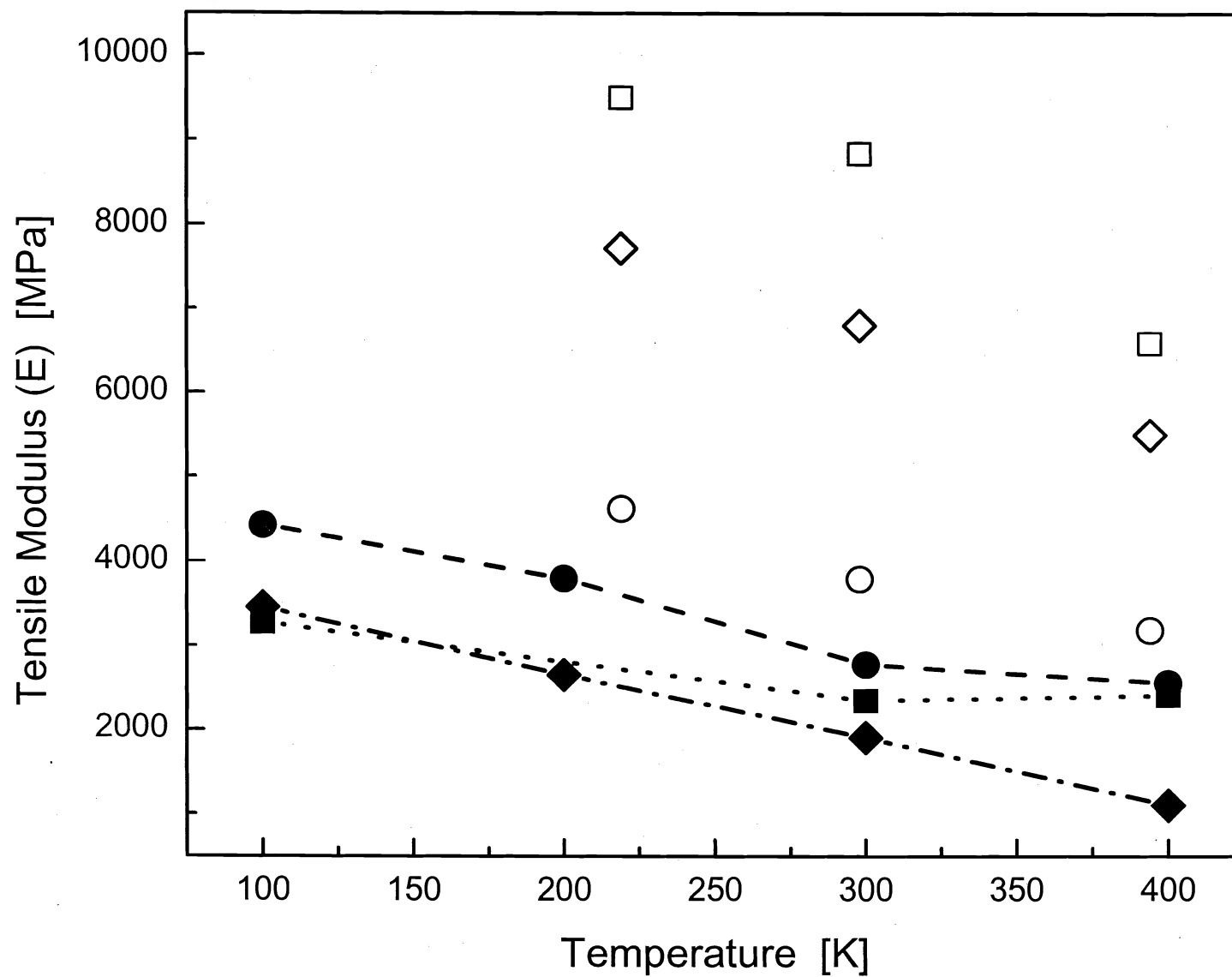Fig. 9: Comparison of Calculated and Experimental Moduli in Parmax SRPs

Fig. 10: Calc'd. Yield Stresses (at 10% Strain) of Parmax SRPs